Journal of Sedimentary Research

Journal of Sedimentary Research, 2019, v. 89, 416–439
Research Article
DOI: http://dx.doi.org/10.2110/jsr.2019.24

PLIOCENE PALEOENVIRONMENTS IN THE MEADE BASIN, SOUTHWEST KANSAS, U.S.A.

WILLIAM E. LUKENS,[1,2] DAVID L. FOX,[3] KATHRYN E. SNELL,[4] LOGAN A. WIEST,[2] ANTHONY L. LAYZELL,[5] KEVIN T. UNO,[6] PRATIGYA J. POLISSAR,[6] ROBERT A. MARTIN,[7] KENA FOX-DOBBS,[8] AND PABLO PELÁEZ-CAMPOMANES[9]

[1]*School of Geosciences, University of Louisiana at Lafayette, Lafayette, Louisiana 70504, U.S.A.*
[2]*Terrestrial Paleoclimatology Research Group, Department of Geosciences, Baylor University, Waco, Texas 76798, U.S.A. and Mansfield University of Pennsylvania, Department of Geosciences, Mansfield, Pennsylvania 16933, U.S.A.*
[3]*Department of Earth Sciences, University of Minnesota, Minneapolis, Minnesota 55455, U.S.A.*
[4]*Department of Geological Sciences, University of Colorado, Boulder, Colorado 80309, U.S.A.*
[5]*Kansas Geological Survey, Lawrence, Kansas 66407, U.S.A.*
[6]*Division of Biology and Paleo Environment, Lamont Doherty Earth Observatory of Columbia University, Palisades, New York 10964, U.S.A.*
[7]*Department of Biological Sciences, Murray State University, Murray, Kentucky 42071, U.S.A.*
[8]*Department of Geology, University of Puget Sound, Tacoma, Washington 98416, U.S.A.*
[9]*Department of Paleobiology, National Museum of Natural History, Madrid, Spain*

ABSTRACT: **Terrestrial paleoenvironmental reconstructions from the Pliocene Epoch (5.3–2.6 Ma) of the Neogene Period are rare from the North American continental interior, but are important because they provide insight into the evolutionary context of modern landscapes and ecological systems. Pliocene marine records indicate that global climate was warmer and atmospheric pCO_2 was higher than pre-industrial conditions, spurring efforts to understand regional climate and environmental variability under conditions potentially analogous to future warming scenarios. In this study, we investigate sedimentary environments and paleoclimate conditions from the Meade Basin of southwest Kansas, a moderately sized basin formed from dissolution and withdrawal of deep evaporites. Pliocene intervals of the Meade Basin have yielded classic faunal assemblages representing the early to middle Blancan North American Land Mammal Age (~ 4.5–3.2 Ma). We reconstruct the paleoenvironments using a multidisciplinary approach of lithofacies analysis, paleopedology, and ichnology. The stratigraphic interval we examined is bounded by large-scale, fluvial trunk channels that show paleocurrent trends to the south-southwest—tangential to modern drainages—likely due to local halotectonic subsidence during the Neogene. The stratigraphic interval between these fluvially dominated phases consists of palustrine landscapes with temporally and laterally variable subaqueous and subaerial facies. Paleosols are abundant; however, most pedotypes are poorly to variably drained, and so their elemental compositions do not reflect local climate state. The few mature, oxidized, and relatively well-drained paleosols observed contain elemental signatures consistent with subhumid climate conditions. Frequent and recursive ponding events are discerned through the tiering of burrows (*Camborygma* isp.) similar to those produced by modern freshwater decapod crustaceans (i.e., crayfish). The drivers of these flooding events are most likely episodic halotectonic subsidence and groundwater discharge, though influence from intervals of relatively wetter climate cannot be ruled out. By the late middle Pliocene, landscapes returned to fluvially dominated environments as sedimentation began to outpace accommodation. Our results collectively indicate that climate was likely wetter than modern conditions in the early to middle Pliocene in the western Great Plains, contrary to forecasts for the region under current pCO_2-driven warming.**

INTRODUCTION

The Pliocene Epoch (5.3–2.6 Ma) of the Neogene Period was the most recent interval of globally warm climates and is a valuable case study for future warming scenarios (IPCC 2014). Paleogeography was similar to modern conditions (Eaton 2008; De Schepper et al. 2015; Montes et al. 2015) and atmospheric pCO_2 is estimated to be 350–450 ppmv (Franks et al. 2014; Royer 2016), which is above preindustrial values (280 ppmv; e.g., MacFarling Meure et al. 2006). However, in contrast to current forecasting models that predict drying of the Great Plains under increased pCO_2, the southwest United States appears to have been wetter in the Pliocene, possibly due to forcing from sea-surface temperature patterns in the equatorial Pacific (Winnick et al. 2013; Ibarra et al. 2018). The need for understanding ecological and landscape response to future warming is confounded by a paucity of quantitative paleoclimate records from the Pliocene of the North American continental interior (e.g., Pound et al. 2014).

The Meade Basin of southwest Kansas (Fig. 1) preserves a rich fossil record from the late Miocene to the Holocene (Honey et al. 2005; Martin et al. 2008; Fox et al. 2012a; Martin and Peláez-Campomanes 2014). Fossil assemblages have been studied from Meade Basin outcrops for nearly a century (see reviews in Zakrzewski 1975 and Martin et al. 2000), and are

Published Online: May 2019
 1527-1404/19/089-416

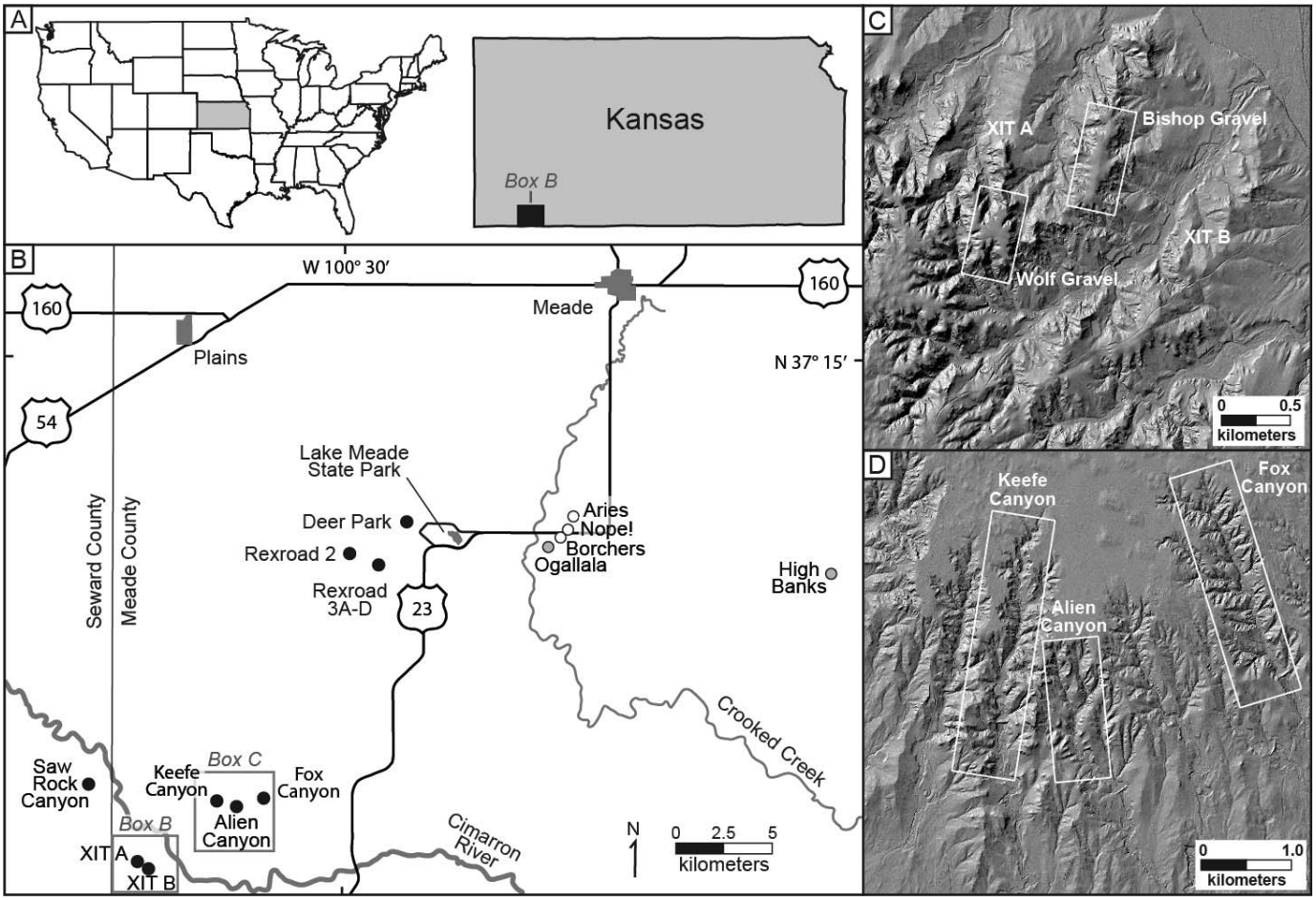

FIG. 1.—**A**, **B)** Fossil localities and study sites in the Meade Basin, southwest Kansas. The current study focuses on localities in C and D. Ages of fossil sites are coded as follows: white circles, Quaternary; black circles, Pliocene; gray symbols, Miocene.

unique in both the constrained geographic extent (Fig. 1) and their relatively high density through the Pliocene and Pleistocene compared to other coeval Great Plains sites (Fig. 2).

Recent investigations into the geological and paleobiological archives of the Meade Basin have revealed new insights into the evolutionary trajectories of climate and biota since the late Neogene. Throughout the Pliocene, the stable-carbon-isotope composition ($\delta^{13}C$) of carbonates gradually increased from –4.9 to –2.6‰ (VPDB), which has been interpreted as an increase from roughly 30 to 50% C_4 grass (Fox et al. 2012a). Corresponding oxygen-isotope ratios ($\delta^{18}O$) from carbonates do not covary with $\delta^{13}C$, suggesting that C_4 grasses did not arise from a simple increase in aridity (Fox et al. 2012b).

Previous work in the Meade Basin interpreted most of the Pliocene intervals as paleosols (fossil soils), and the carbonate components as pedogenic nodules and calcretes (Fox and Koch 2003; Retallack 2007; Fox et al. 2012a, 2012b). Here we analyze paleosols and sedimentary deposits to reconstruct paleogeomorphic and postdepositional processes that are critical for assessing styles of pedogenesis and discerning pedogenic products from other superficially similar features. This analysis is critical for accurate interpretation of stable-isotope records from carbonates and sedimentary organic matter, as formation mechanism and provenance are important factors that can affect stable-isotope paleoclimate proxies.

In this investigation, we first document the stratigraphy and sedimentology of the study area, with depositional units organized in a lithofacies framework. Geomorphic and climatic information preserved in paleosols are assessed using morphological and elemental analysis of pedotypes. Transfer functions that relate elemental composition of paleosol B horizons to climate conditions were evaluated and the results are placed into context in the geologic setting for the Meade Basin. Finally, we propose a facies model that incorporates observations from lithofacies associations, paleosol distributions, and ichnological tiering. The stratigraphic sections under study were used previously to generate stable-isotope paleoclimate proxy records (Fox et al. 2012a, 2012b) and are the subject of ongoing stable-isotope work that is beyond the scope of this study.

GEOLOGIC SETTING

Meade Basin Stratigraphy

The Meade Basin in southwest Kansas formed as the result of salt dissolution and withdrawal from underlying Permian evaporites (Frye and Schoff 1942; Merriam and Mann 1957; Seni 1980; Gustavson 1986). Sediments eroded off the Rocky Mountains were deposited in the Central High Plains, which includes the Meade Basin, beginning as early as the Paleogene (Smith et al. 2017). Modulation between uplift, erosion, and isostatic compensation have maintained a shallow (hundreds of meters thick) veneer of sediments in the area since the Neogene (Leonard 2002), and therefore the Meade Basin was not subjected to significant burial diagenesis. Fluvial gravels of the Miocene Ogallala Formation are exposed at several Meade Basin sections, though most areas contain Pliocene to Holocene sedimentary units (Fig. 1). We focus here on exposures of early

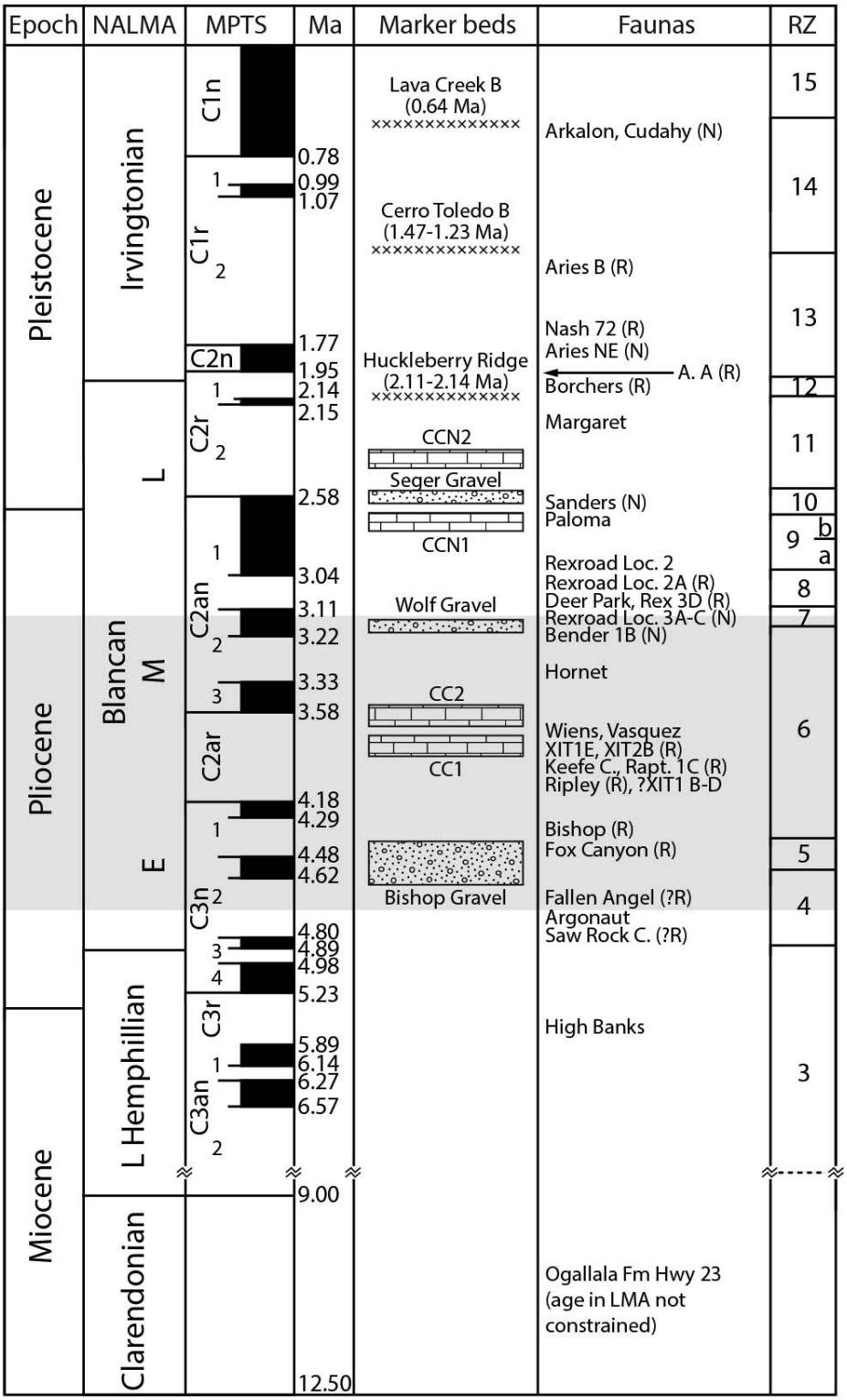

FIG. 2.—Composite stratigraphy for the Meade Basin, Kansas. Magnetostratigraphy is based on paleomagnetic analysis of Lindsay et al. (1975). Gray shading indicates the study interval for this investigation. NALMA, North American Land Mammal Age; MPTS, Magnetic Polarity Time Scale, with normally polarized chrons identified with black bars; RZ, rodent zones, after Martin (2003).

Pliocene strata in dry canyons of ephemeral steams that are tributaries of the Cimarron River. We use the stratigraphic framework of Honey et al. (2005), in which stratigraphic sections are correlated using conspicuous gravel and carbonate units as marker beds (Figs. 2, 3). Earlier researchers referred to Pliocene strata along the Cimarron River as the Rexroad Formation (Hibbard and Riggs 1949; Hibbard 1950); we follow Honey et al. (2005) in avoiding formal lithostratigraphic nomenclature for these strata because correlations to the Rexroad Formation type locality have yet to be demonstrated.

Age control is based on well-resolved biostratigraphy based primarily on fossil rodent assemblages coupled with magnetostratigraphy (Lindsay et al. 1975; Martin 2003; Martin et al. 2008). Evolutionary trends and

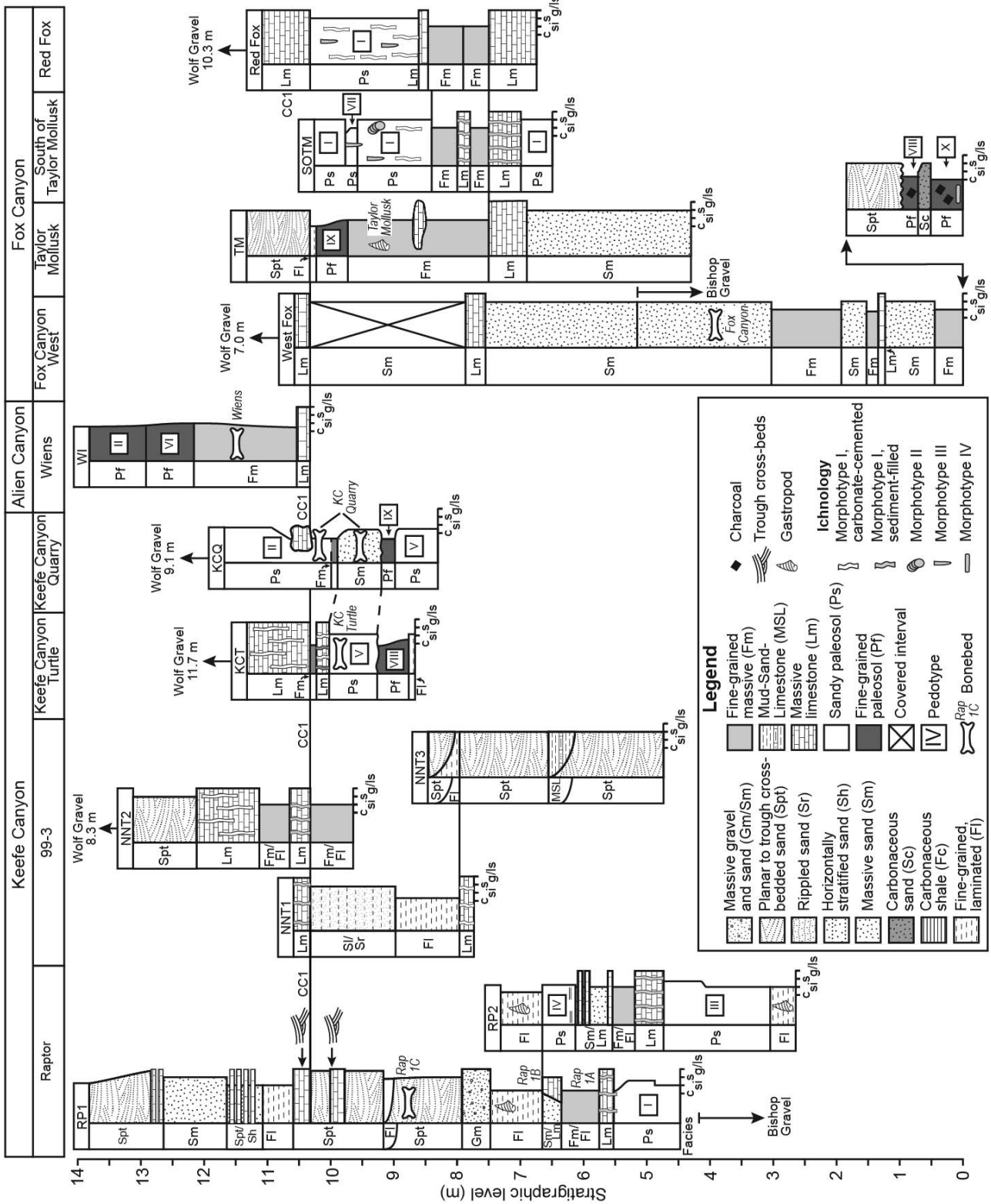

FIG. 3.—Stratigraphic sections from sites north of the Cimarron River. Names of localities (canyons) and sections are listed along top panel. Section abbreviations are identified above each stratigraphic column. Horizontal lines between sections identify lateral correlations. See Table 2 for lithofacies, Figure 6 for pedotypes, and Table 4 for ichnological morphotypes. Stratigraphic thickness to Wolf Gravel is noted where intervening stratigraphy was not exposed.

community changes in these fossil assemblages have been documented as part of the Meade Basin Rodent Project (Peláez-Campomanes and Martin 2005; Marcolini and Martin 2008; Martin et al. 2011; Martin and Peláez-Campomanes 2014; Goodwin and Martin 2017). Faunal sites associated with the outcrops near the Cimarron River contain classic Blancan taxa and have been arranged into a rodent biostratigraphy using arvicolid index taxa by Martin (2003) (Fig. 2). The stratigraphic interval we examined includes the late early Blancan (4.5–4.0 Ma; Bell et al. 2002), defined by the presence of *Pliophenacomys finneyi* in the Fox Canyon assemblage (Hibbard 1950; Hibbard and Zakrzewski 1972) and the early to middle Blancan species *Ogmodontomys poaphagus* (4.0–2.8 Ma) in sites in Fox and Keefe canyons and at the Wiens site (Honey et al. 2005; Marcolini and Martin 2008). The Wolf Gravel caps the study interval and has an inferred age of $\sim$ 3.2–3.1 Ma (Fig. 2) based on magnetostratigraphy (Lindsay et al. 1975), biostratigraphy (Martin 2003), and stratigraphic correlations of Honey et al. (2005).

Meade Basin Rodent Paleontology

Fossil rodent communities in the Meade Basin allow climatic and environmental interpretations independent of geologic archives based on taxonomic uniformitarianism (Peláez-Campomanes and Martin 2005; Martin et al. 2008; Martin and Peláez-Campomanes 2014; Goodwin and Martin 2017). All unambiguously identified rodent species from early to middle Pliocene (4.5–3.2 Ma) assemblages are extinct (Figs. 1, 2; Martin and Peláez-Campomanes 2014). However, fossil assemblages in the basin throughout the late Cenozoic include persistent modern prairie components, such as ground squirrels, pocket gophers, kangaroo rats, pocket mice, grasshopper mice, and pygmy mice (Martin and Peláez-Campomanes 2014). General climatic conditions can be inferred by presence/absence data. For example, some of the Blancan ground squirrels (*Otospermophilus*, *Ammospermophilus*) represent a southwestern biogeographic component that contrasts with younger taxa predominantly in the High Plains today (e.g., *Urocitellus*, *Cynomys*, *Poliocitellus*, *Ictidomys tridecemlineatus*). These differences suggest early Pliocene aridity, as *Ammospermophilus* is today restricted to desert environments (Goodwin and Martin 2017).

Multiple extant species of cotton rats (*Sigmodon*) are distributed in riparian habitats ranging from Arizona to the Atlantic coast and south through Mexico to northern South America. Additionally, *S. hispidus* can be locally extirpated during harsh winters in the northern part of its range in central and eastern U.S.A., partly because they do not reproduce under the snow and cannot accumulate enough fat to survive long, extreme winters (Slade et al. 1984). Cotton rats of various species are present intermittently in the Meade Basin record, suggesting the presence of riparian habitats and absence of extreme winters. Tentatively, the rodent assemblages suggest that the Meade Basin has remained a prairie mosaic, punctuated by both arid and mesic (and likely warmer) periods with attendant shifts in plant community composition.

PALEOSOLS AS PALEOENVIRONMENTAL ARCHIVES

A primary objective of this study is to interpret paleoclimate influences on the formation of paleosols during the Pliocene in the Meade Basin. We follow the state-factor framework for pedogenesis (Jenny 1941, 1994):

$$S \text{ or } s = f(cl, o, r, p, t, \ldots) \quad (1)$$

where S is soil and s is any soil feature, both of which form as a function of climate (cl), organisms/biota (o), topographic relief (r), parent material type (p), and time/duration of pedogenesis (t). The ellipsis signifies errors imparted by unknown or additional influences on S or s (e.g., dust influx or water-table fluctuation; Holliday 2004). While all state-factors interact to generate a soil, some geologic settings allow individual factors to dominate over the others (Jenny 1994; Holliday 2004). For example, soils formed over short durations tend not to be in geochemical equilibrium with climate, and soils with pre-weathered parent materials can inherit a climatic signal thereby appearing to have formed in hotter and wetter climates than those under which they actually formed (Yaalon 1971; Stinchcomb et al. 2016). In paleopedological studies of paleoclimate, ideal paleosols maximize the expression of climate in geochemical trends or morphological properties and are not dominated by signals imparted by state-factors that do not covary with climate.

METHODS

Field Methods

We studied 13 stratigraphic sections with established lithostratigraphic frameworks (Honey et al. 2005) and well-studied vertebrate faunas that indicate the sections correspond to the early to middle Blancan North American Land Mammal Age (ca. 4.5–3.2 Ma) (Fig. 2; Hibbard and Riggs 1949; Hibbard 1950; Lindsay et al. 1975; Honey et al. 2005; Martin et al. 2008). All outcrops in this study were redescribed for stratigraphic correlation, facies analysis, and detailed paleosol analysis. Correlation between measured sections was accomplished in each locality by walking out marker beds or using a hand-held transit compass. Correlation between localities is based on the use of two conspicuous gravel units as marker beds (the Bishop and Wolf gravels) that act as caprocks, where present, in many stratigraphic sections.

Lithofacies were assigned using standard nomenclature (Miall 1978, 2013) and methods similar to recent sedimentology studies at other Neogene localities in the Great Plains (Joeckel et al. 2014; Lukens et al. 2017a). Sedimentary deposits exhibiting soil features (paleosols) were described using a modification of U.S. Department of Agriculture–Natural Resources Conservation Service (USDA-NRCS) field methods (Schoeneberger 2002), and include observations of horizonation, ped structure, color, authigenic and translocated minerals, grain size, bounding contacts, root traces, and invertebrate trace fossils, where present. Pedotypes were delineated using a combination of observed sedimentologic and pedogenic features from descriptions of individual paleosol profiles (*sensu* Retallack 1994). Trace fossils were grouped as morphotypes based on surficial and architectural morphology, tiering, orientation, host matrix, infilling material, and dimensions.

Laboratory Methods

Serial samples were collected in the field every 10–20 cm from nine paleosol profiles and prepared and analyzed at Baylor University. Bulk samples were ground and homogenized using a shatterbox. Loss on ignition (LOI) was measured as the mass loss between oven drying (110°C for 24 hr) and roasting in a muffle furnace (550°C for 2 hr) (Lukens et al. 2016b). Samples were then fused into glass pucks using Li-borate flux and analyzed for elemental concentrations using a Rigaku ZSK Primus II X-ray fluorescence (XRF) analyzer. Repeated analyses of standards resulted in a relative standard deviation of 0.01–0.05 wt. % for all oxides.

Thin sections were analyzed from the uppermost B horizon of three paleosols that span the range of morphological associations observed in the field. These include the Bk horizon of a well-drained, oxidized, sandy paleosol (Pedotype 1; see Paleopedology section, below), the Bkssg horizon of a redoximorphic, calcic, fine-grained paleosol (Pedotype VIII), and the Bg horizon of an aquic, non-calcic, fine-grained paleosol (Pedotype X). These horizons were selected for micromorphologic analysis because they typify macroscopic evidence of well drained, variably drained, and poorly drained conditions (respectively). Micromorphological observations focused on the presence and degree of silicate mineral weathering, clay and carbonate authigenesis, redistribution of clays, redoximorphic mineral transformations, and bioturbation by invertebrates

TABLE 1.—*Paleosol proxies for paleoclimate.*

Index	Index Formula	Model Error*	Constraints	Reference
Mean annual precipitation				
CIA-K	$221.1e^{0.0197(\text{CIA-K})}$	181 mm	No Oxisols, Gelisols, or Histosols	Sheldon et al. 2002
Mean annual temperature				
NaK	$-18.5x + 17.3$	4.4°C	No Oxisols, Gelisols, or Histosols	Sheldon et al. 2002
Mean annual precipitation and temperature				
PPM	Thin plate spline**	512 mm, 3.98°C	Uppermost B horizons; no Gelisols	Stinchcomb et al. 2016

Note: Formulas for the CIA-K and CALMAG indices are included in the text.

* Values used are standard errors from regression analysis, except for PPM, which are root-mean-square prediction errors based on validation modeling. Error for CIA-K is from Sheldon and Tabor (2009).

** Modeled in SAS statistical software; see Stinchcomb et al. (2016) for code and methods.

and vegetation using methods from Brewer (1964) and Bullock et al. (1985).

Paleoclimate Estimations

The elemental composition of B horizons was used to estimate mean annual precipitation (MAP) and temperature (MAT) using pedotransfer functions calibrated on modern North American soils (Sheldon et al. 2002) (Table 1). The chemical index of alteration minus potassium (CIA-K = 100 × [Al_2O_3 / (Al_2O_3 + CaO + Na_2O)]) is used as a predictor in an exponential transfer function for MAP. The CIA-K proxy is sensitive to MAP due to 1) calcium carbonate precipitation in drylands, which buffers against mobile base loss, and 2) progressive silicate hydrolysis, decarbonation, and competition of H^+ and Al oxyhydroxides for colloidal exchange sites in wetter climates (Sheldon et al. 2002; Lukens et al. 2018). MAT was predicted by a linear pedotransfer function based on the salinization index (NaK = [(Na_2O + K_2O) / Al_2O_3]), which tracks the thermodynamic dissolution of feldspars as a function of temperature (Sheldon et al. 2002) and is possibly sensitive to salt accumulation under dry-cold climates (Sheldon and Tabor 2009).

The paleosol–paleoclimate model version 1.0 ($PPM_{1.0}$, Stinchcomb et al. 2016) was also used to co-predict MAP and MAT. The $PPM_{1.0}$ uses eleven elemental oxides as inputs (Fe_2O_3, Al_2O_3, SiO_2, TiO_2, ZrO_2, CaO, MgO, K_2O, Na_2O, MnO, and P_2O_5) to model both MAP and MAT using a thin-plate spline drawn through sample scores generated by a partial least-squares regression analysis of modern uppermost B horizon soil samples. Although MAP prediction errors are greater for the $PPM_{1.0}$ than for CIA-K, a larger variety of soils were used for calibration of the $PPM_{1.0}$ model, which should allow prediction of climate from paleosols formed under a wider range of environmental conditions. The $PPM_{1.0}$ was run in SAS statistical software (SAS Institute, Inc., v. 9.2.).

Paleocurrent Analysis

Azimuthal trend of trough cross-beds was measured in the field on plan-view outcrops of bedding planes in fluvial channel sandstones. Statistical analysis of current directions was performed in Stereonet 10.0 (Allmendinger 2018). Mean vectors for trends in each group were calculated as the mean orientation of the Fisher vector distribution, which is the mean direction cosine of individual unit vectors (Fisher 1953; Fisher et al. 1987).

LITHOFACIES

Lithofacies codes, diagnostic features, and environmental interpretations are presented in Table 2. We identified 14 lithofacies that ranged from clast-supported gravel to laminated clay. The stratigraphy of our sections is shown in Figure 3 (sections north of the Cimarron River) and Figure 4 (the XIT Ranch section south of the Cimarron River).

TABLE 2.—*Lithofacies and environmental interpretations.*

Code	Lithofacies	Sedimentary Structures	Interpretation
Gm	Gravel	Massive to trough cross-bedded	Gravel bar in bedload-dominated channel
Spt	Medium to vc sand, gravel at base	Planar and trough cross-bedding; scours possible at base of units	Suspended-load fluvial channel
Sh	Sand, horizontal stratification	Horizontal stratification	Suspended-load fluvial channel
Sm	Massive sandstone	Structureless, but lacks pedogenic features	Bioturbated fluvial or lacustrine sand
Sc	Carbonaceous sandstone	Organic-rich sandstone, typically with carbonized root traces and/or charcoal; massive to ripple-laminated	Crevasse splay
Fl	Fine-grained, laminated	Weakly laminated to massive; mollusk shells	Palustrine or wetland
Fm	Fine-grained, massive	Lacks sedimentary and pedogenic structure; may contain invertebrate burrows or rare root traces	Bioturbated palustrine or wetland
Fc	Carbonaceous shale	Organic-rich shale, typically with carbonized root traces and/or charcoal; laminated	Swamp or wetland
MSL	Mudstone, sandstone, limestone	Thin bedding to laminated, mudcracks	Slackwater in fluvial channel
Lm	Massive limestone with burrows	Massive; *Camborygma* isp., wavy contacts, lacks pedogenic features	Evaporative palustrine, restricted water body
Ps	Sandy paleosol	Structureless, contains root traces and variable pedogenic structure and carbonate nodules	Sandy paleosol (see pedofacies)
Pf	Fine-grained paleosol	Pedogenic structure, root traces, variable mineralizations, variable color	Fine-grained paleosol (see pedofacies)

Note: Facies codes are modified from Miall (1978). Sand sizes: vf (very fine), f (fine), m (medium), c (coarse), vc (very coarse).

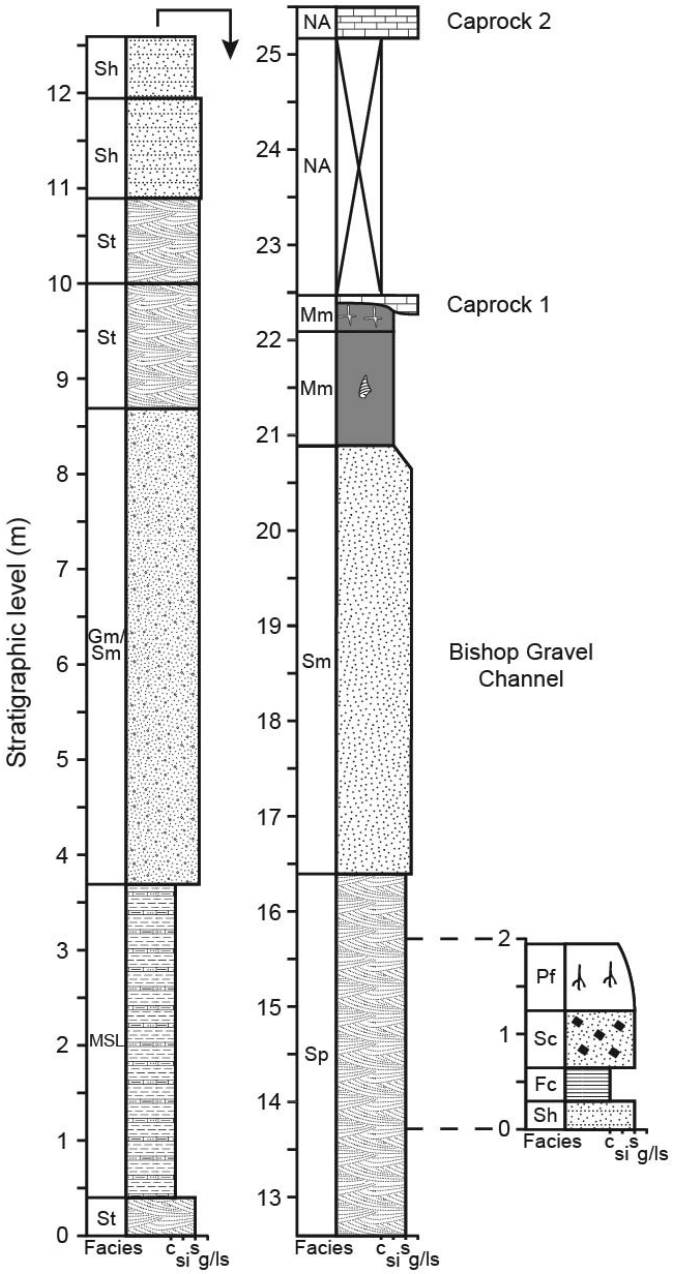

FIG. 4.—Stratigraphic section XITB, measured at XIT Ranch south of the Cimarron River. The Bishop Gravel (ca. 16.5–21 m in section) correlates to the base of the stratigraphic successions in Figure 3. See Figure 6 for pedotypes. Small lateral section (ca. 13.8–15.8 m in section) was described roughly 100 m east of the main column.

Gravel Units

Observations of Gravels.—Two gravel units observed in the study area typically occur as caprock units where present and consist of poorly sorted, clast-supported, interbedded conglomerates and gravelly, lithic, medium to coarse sandstone (Gm). These units are best exposed at XIT Ranch (Fig. 5A). The Bishop Gravel occurs at the base of sections north of the Cimarron River (Fig. 3) and near the base of the sections at XIT Ranch (Fig. 4, 5A). The Wolf Gravel is the dominant caprock at XIT Ranch (Fig. 5A–C) and is visible above covered intervals in sections north of the Cimarron River. Both units are gravelly sublitharenites and are differentiable based on granite being the modal clast $>$ 2 mm in the Wolf Gravel ($\sim$ 30% overall) and quartzite the most common in the Bishop Gravel ($\sim$ 27% overall). Both units contain accessory igneous, metamorphic, and sedimentary lithics. Sedimentary structures include meter-scale planar to tabular cross-stratification and horizontal bedding (Fig. 5B–E).

TABLE 3.—*Trunk-channel paleocurrents*.

Locality	Mean*	Error**	n
Bishop Gravel			
XITB	181	8.0	25
Keefe Canyon	241	13.2	6
All Bishop localities	192	8.2	31
Wolf Gravel			
XITB	139	35.2	10
Keefe Canyon	213	11.2	12
All Wolf localities	195	16.0	22
All measurements	193	7.7	53

Note: All measurements were taken from trough cross-beds.
* Mean orientation of Fisher vector distribution
** 1σ error of mean value.

Paleocurrent directions for the Bishop and Wolf gravels are oriented south-southwest (Table 3). The Watson U^2 test (the analogue of the Mann-Whitney U test for non-directional data) on the azimuthal data indicates that directions are not significantly different between the Wolf and Bishop gravels when all localities are grouped by stratigraphic position ($U^2 = 0.075$, $0.20 < p < 0.50$). However, at Keefe Canyon, paleocurrent directions for the two Gm units are significantly different ($U^2 = 0.293$, $p < 0.01$).

Interpretations of Gravels.—The Gm lithofacies is interpreted as bedload-dominated, fluvial trunk channels based on the coarse, clast-supported matrix and presence of 2D and 3D dunes. Cross-sectional and plan-view exposures of the channels indicate that the channels were generally straight with low to moderate sinuosity, and paleocurrents indicate that flow was oblique to the modern Cimarron River (Fig. 5A–F).

Sandstones

Observations of Sandstones.—Lenticular beds of moderately well sorted, medium sandstone to moderately poorly sorted, very coarse sandstones contain decimeter- to meter-scale tabular and trough cross-bedding and horizontal stratification (Spt). Successions of Spt units have internal depositional packages ranging from 1 m to 2 m thick with flat to scoured bases and flat upper contacts, and are typically juxtaposed with other Spt units or fine-grained facies (Fig. 5H).

Sandstones with planar lamination (Sl) are interbedded with ripple-laminated sandstones (Sr), each of which occur as depositional units generally $<$ 1 m thick. Massive, well-sorted fine sandstones to clayey fine sandstones that lack pedogenic features (Sm) tend to be tens of centimeters thick. The lower part of the Keefe Canyon Quarry fossil assemblage occurs in an Sm unit. Massive sandstones with pedogenic features (Ps) are subdivided into pedotypes (see below).

Sandstone Interpretations.—The Spt lithofacies is interpreted as sand-dominated fluvial channels based on lenticular cross sections, upper flow regime plane beds, and 2D and 3D ripples to dunes (Bridge 2003). Internal depositional packages in Spt units are interpreted to be channel stories

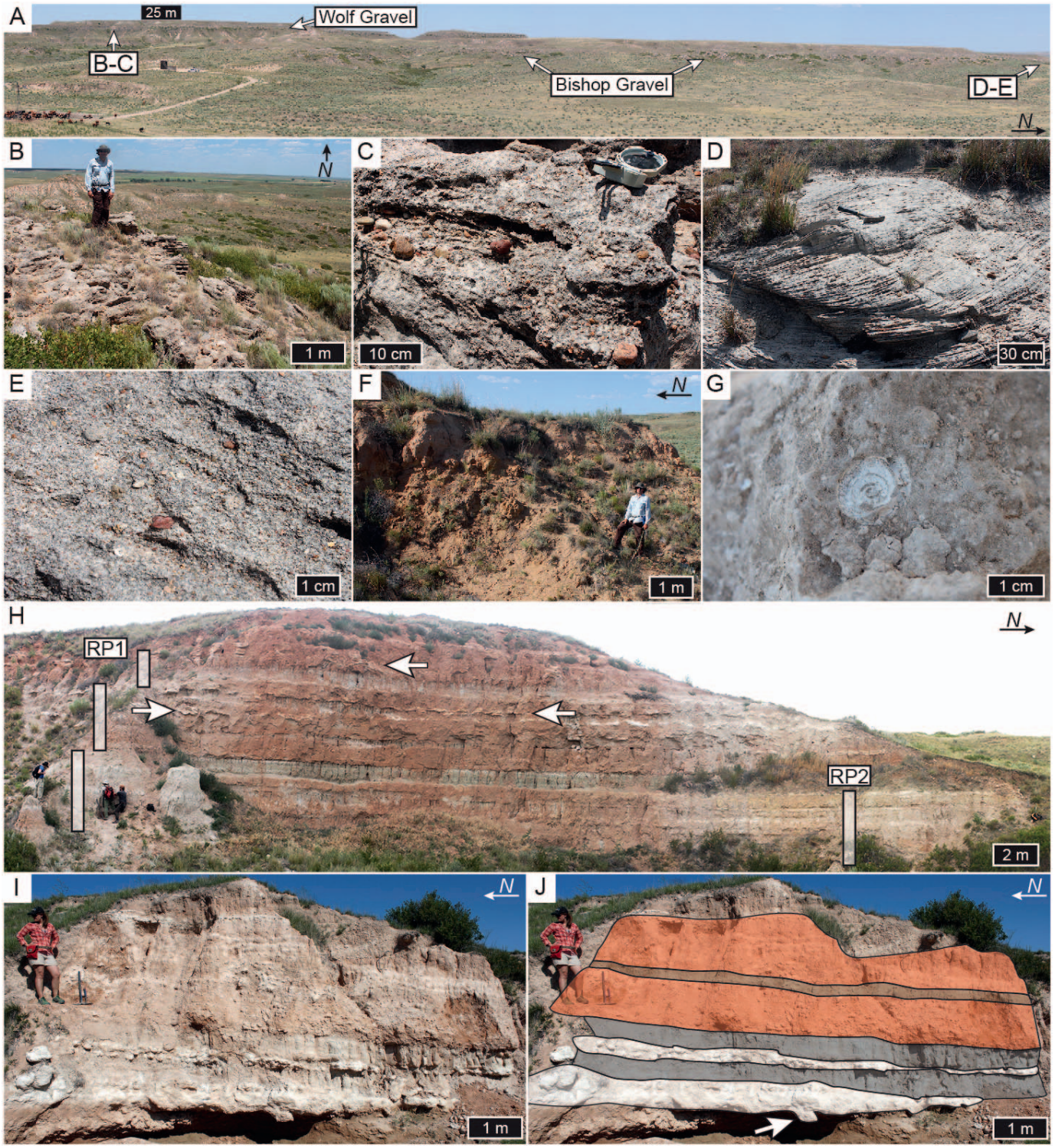

FIG. 5.—Macroscopic lithofacies features. **A)** The Bishop and Wolf Gravel units form resistant ledges, oriented generally north–south, at XIT Ranch. **B)** Wolf Gravel outcrop, with trough cross-bedded, gravelly sandstones. **C)** Wolf Gravel composition, consisting of sublitharenite sandstone with floating granite and quartzite pebbles. **D)** Bishop Gravel outcrop, with large 3D dunes oriented south-southwest. **E)** Bishop Gravel composition, consisting of sublitharenite sandstone with floating granite and quartzite gravel. **F)** Highly weathered outcrop of Bishop Gravel in Keefe Canyon, near the Raptor outcrop (see Fig. 3). **G)** Gastropod in Fm lithofacies. **H)** Raptor outcrop in Keefe Canyon. Vertical boxes identify stratigraphic sections RP1 and RP2. White arrows identify carbonates precipitated along trough cross-beds in fluvial channels. Green recessed strata are Fm lithofacies. **I**, **J)** South of Taylor Mollusk outcrop in Fox Canyon, with lithofacies units delineated. White intervals are Lm lithofacies; note Morphotype I (*Camborygma* isp.) crosscutting lower boundary (white arrow in Part J). Gray intervals are Fm lithofacies. Orange intervals are Ps lithofacies/Pedotype I. Brown stripe identifies Pf lithofacies/Pedotype VII.

based on erosional contacts with underlying units. Most channels are multistoried.

Interbedded Sl and Sr units occur only in the 99-3 section (NNT1, Fig. 3). The interval is lateral to a fluvial channel in the Raptor section and represents fluvial sedimentation into a shallow floodplain pond (e.g., Toonen et al. 2012).

The Sm lithofacies is featureless, and therefore possibly formed through multiple pathways. The lack of bedding is attributed to cryptic bioturbation and incipient pedogenesis in some units. In the Fox Canyon West and Taylor Mollusk sections, Sm units are likely Spt units that have experienced modern weathering, as they are very thick, have floating gravels, and have been previously interpreted as the Bishop Gravel channel (Honey et al. 2005). In the Keefe Canyon sections, Sm units are either shallow palustrine or proximal fluvial deposits, the primary depositional features of which were obscured by bioturbation. We note, however, that individual trace fossils were not observed in these units.

Fine-Grained Facies

Observations of Fine-Grained Facies.—Fine-grained units with laminae (Fl) and massive, bioturbated deposits (Fm) vary from sandy or silty clay to clayey siltstone, lack evidence of pedogenic modification, and tend to be < 1 m thick. Features include gastropod shell fragments and external molds, charcoal, and organic-rich mud (Fig. 5G, I, J). The vertebrate fossil assemblages Raptor 1A, 1B, and the upper part of the Keefe Canyon Quarry assemblage all occur in Fm or Fl deposits (Fig. 3). Matrix color of these units varies from dark brown to greenish brown to gray, and root traces are rare to absent. These units typically overlie Lm lithofacies (see below) and contain vertical to subhorizontal, unlined, passively filled burrows. Other fine-grained units that contained pedogenic features (Pf) were subdivided by pedotype (see below).

Interpretations of Fine-Grained Facies.—The Fl lithofacies is interpreted as pond deposits based on the presence of organic-rich, laminated clays and mollusk fossils. Fm lithofacies are generally similar but lack bedding, have slightly coarser grain size, and are lighter in color, presumably due to less organic matter. The Fm lithofacies is interpreted to be siliciclastic infill of ponds. Where Fm units are interstratified with facies interpreted as palustrine units (e.g., bioturbated Lm units; see Limestones section, below), we interpret them as siliciclastic palustrine facies (e.g., Taylor Mollusk, South of Taylor Mollusk, and Red Fox sections; Fig. 3). Where Fm units occur next to or juxtaposed with fluvial channels (Spt) or oxbow-lake infill (MSL), we interpret them as bioturbated, late-stage infilling of oxbow lakes (Toonen et al. 2012).

Limestones

Observations of Massive Limestones.—The massive limestone (Lm) lithofacies occurs as white, dominantly micritic limestone with no observable bedding and is used exclusively for units that are not associated with pedogenic carbonate accumulation (Fig. 5I, J). In some areas, the limestone intermittently transitions to weakly cemented, fine to medium sandstone. Lower contacts are abrupt with variably smooth, irregular, or nodular topography. Upper contacts are abrupt and smooth. Micritic limestones contain well-rounded, fine to medium quartz grains floating in an otherwise massive matrix. Vertical, smooth-walled, unlined burrows commonly crosscut Lm deposits and are passively filled with brown to gray, fine, sandy siltstone from overlying Fm deposits. Nodular zones along lower contacts are associated with small (1–2 cm wide), carbonate-filled, knobby, branching and intersecting burrows penetrating underlying units.

Interpretations of Massive Limestones.—The Lm lithofacies is interpreted to be palustrine limestone based on the common association with Fm deposits and ichnological tiering (see Ichnology section, below). A diagenetic origin is ruled out for Lm carbonates due to the abrupt upper contacts of Lm units with overlying strata, burrows that crosscut the limestone and are filled with sediment of the overlying Fm unit, and the lack of bedding or other relict sedimentary features that would have predated diagenetic cementation.

Observations of Mud–Sand–Limestones.—Laminated mud, sand, and limestone (MSL) occur juxtaposed with the Spt lithofacies. Beds are generally < 1 m thick, although the MSL unit in the XITB section is thicker. The base of MSL units is irregular and non-erosional, and the upper contacts tend to be wavy and eroded by overlying Spt facies.

Interpretations of Mud–Sand–Limestones.—The MSL lithofacies is interpreted to be the laminated slackwater fill associated with oxbow lakes after channel abandonment (Toonen et al. 2012). This interpretation is supported by the lenticular cross-sectional geometry of MSL deposits at the 99-3 outcrop, and the presence of Spt channel sandstones above and below the MSL interval. The thicker MSL unit in the XITB section (Fig. 4) coincides with larger fluvial channels below the level of the Bishop Gravel. The presence of carbonates in the oxbow-filling succession indicates either highly evaporative conditions, seepage of alkaline groundwater, or overland transport of waters rich in Ca^{2+} (e.g., Gierlowski-Kordesch et al. 2013).

PALEOPEDOLOGY

Pedotype profile descriptions and elemental data are available in Tables S1 and S2 (see Supplemental Material). We described 18 paleosol profiles in the field and group them here into ten pedotypes (Pedotypes I through X) (Fig. 6). Each grouping is based on similar macromorphologic features, including horizonation, color, presence of pedogenic minerals, redox features, and grain size. The following observations include diagnostic features of each pedotype followed by interpretations, which include assignment of pedotypes to possible modern soil taxonomic classes. We follow NRCS soil taxonomy (Soil Survey Staff 2014); however, we note that such classifications can be problematic, as many key differentiae are impossible to measure after burial (Mack et al. 1993). For example, Mollisols were excluded as a possible soil order assignment due to the erosion of surface horizons in most profiles. Nevertheless, we classify the pedotypes to the highest possible taxonomic category using their observable features.

Pedotype I

Observations of Pedotype I.—Pedotype I (lithofacies Ps) formed on uniform, red, fine loamy sand and has stacked Bk horizons (Figs. 5I, J, 6A, 7A). The lowermost Bk horizon (Bk3) contains tabular carbonates and radial, bladed molds of salts, likely gypsum or barite. Carbonate morphologies grade upward into irregular masses (Bk2) and discrete nodules and wisps (Bk1), consistent with Stage II carbonate accumulation (Gile et al. 1966) (Fig. 7A). Pedotype I is common throughout Fox Canyon and tends to overlie Lm or Fm units.

Thin-section analysis of the Bk horizon reveals a matrix of fine sand and silt, dominated by quartz and potassium and plagioclase feldspars (Fig. 8A). Authigenic clay is present in association with hydrolyzed feldspars and is redistributed throughout the matrix as birefringent (sepic) fabric. Matrix impregnations (argillans) occur in isolated zones (Fig. 8B). Coatings on detrital skeleton grains and carbonate nodules (granostriated fabric) are common (Fig. 8C). Clay coatings on pores (porostriated fabric) were not observed, nor were any accumulations of Fe or Mn. Pedogenic

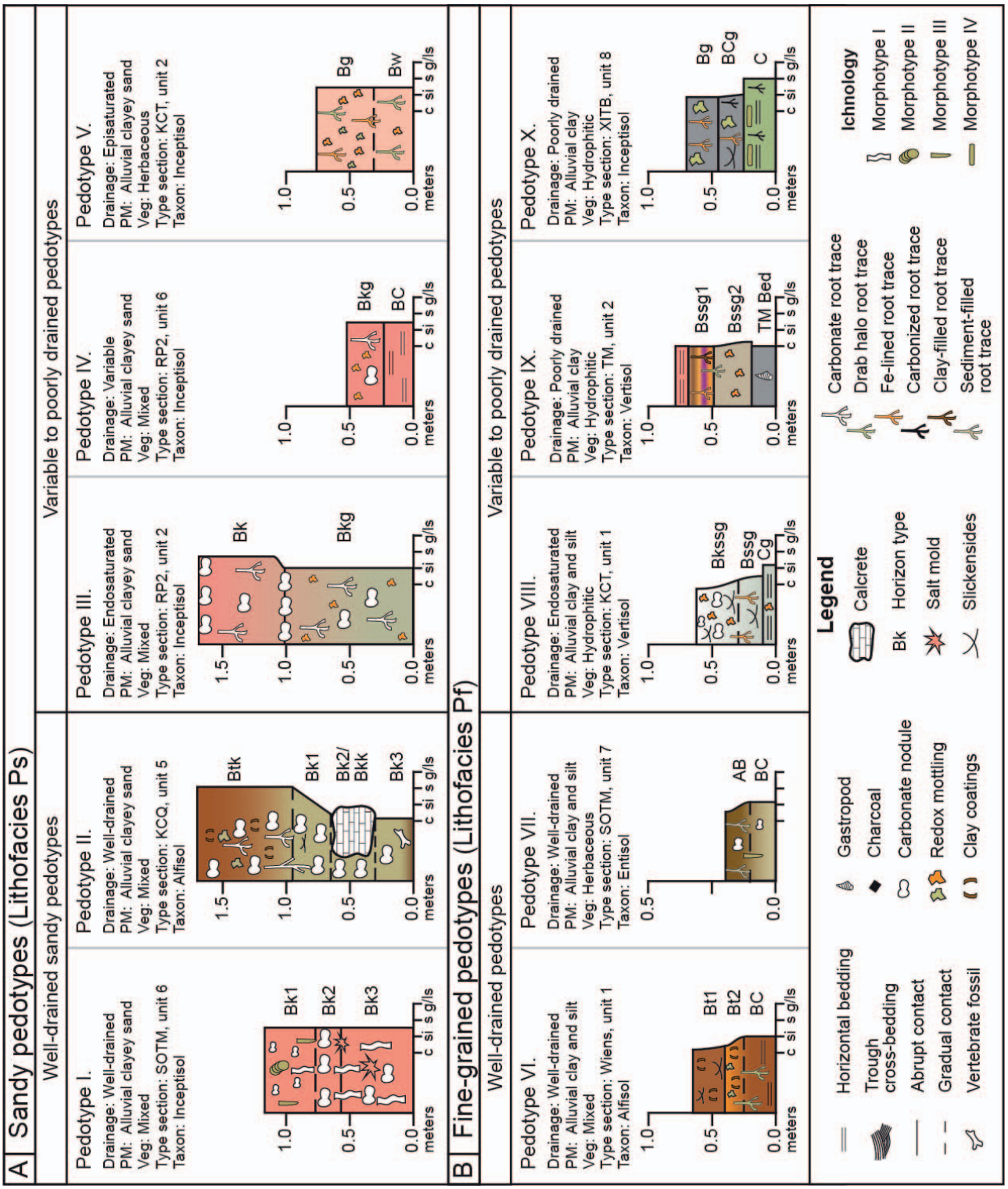

FIG. 6.—Pedotype profiles and basic interpretations. **A)** Sandy pedotypes have predominantly sand texture. **B)** Fine-grained pedotypes have a silt to clay texture. All pedotypes are organized according to drainage characteristics. Note: PM, paleosol parent material type; Veg, inferred vegetation; type sections refer to Figure 3; Taxon, soil order in USDA-NRCS terminology.

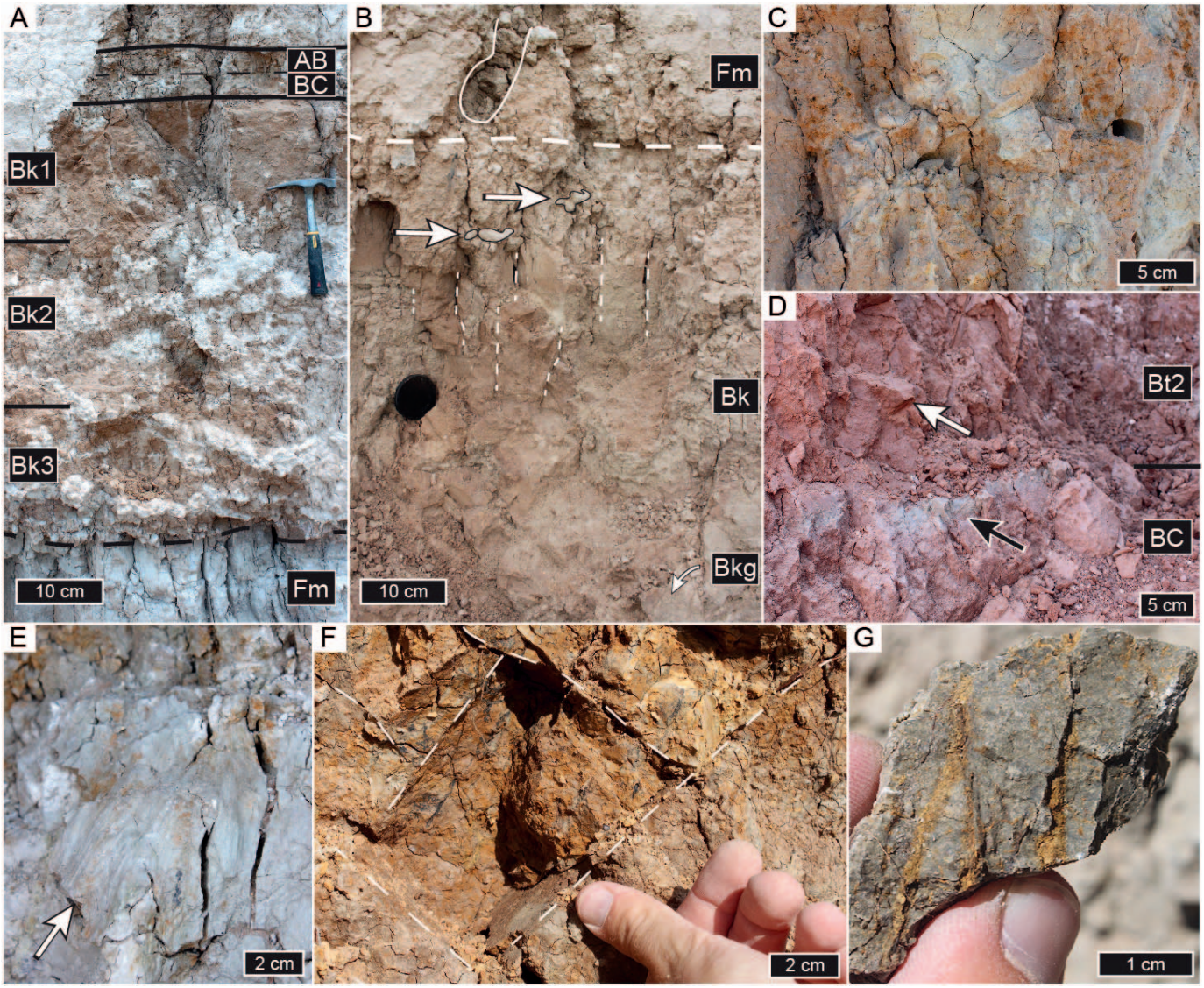

FIG. 7.—Paleosol macroscopic features. **A)** Paleosols in the SOTM section. Pedotype VII (AB, BC horizons) underlain by stacked Bk horizons of the Pedotype I. Tabular phreatic carbonate in Bk3 transitions to filamentous and nodular vadose carbonates in Bk1. Lowest unit is Fm lithofacies. **B)** Pedotype III , overlain by Fm lithofacies (RP2 section). White oval in Fm delineates Morphotype I burrow (*Camborygma* isp.). White arrows identify micrite-filled Morphotype I burrows overprinting the Bk horizon. Thin dashed lines trace prismatic peds; RP2 section. **C)** Redoximorphic Bg horizon from Pedotype V; Keefe Canyon Turtle section. **D)** Pedotype VI from the Wiens section with angular blocky peds (white arrow) and reduction mottling (black arrow). **E)** Bkssg horizon of Pedotype VIII. Note white carbonate nodules and slickenside (white arrow); Keefe Canyon Turtle section. **F)** Wedge peds and slickensides (dashed lines) in Bssg1 horizon of Pedotype IX; Taylor Mollusk section. **G)** Fe-filled root traces and angular blocky ped; Bg horizon of Pedotype X; XITB section.

carbonates occur as micritic masses that incorporate detrital silicate grains (Fig. 8C, D), and they do not exhibit septarian shrinkage cracks or evidence of sparry recrystallization or overgrowths. Root traces and ped boundaries were not observed.

Interpretation of Pedotype I.—The uniform texture of Pedotype I suggests an alluvial parent material with possible eolian inputs. Pedotype I overlies facies interpreted to be palustrine in origin (Fm, Lm), and therefore these paleosols developed on aggradational, emergent land surfaces. The lack of parent-material discontinuities or abrupt changes in sedimentology within the profiles of Pedotype I indicates that soil formation kept pace with sedimentation, resulting in cumulative profiles (Kraus 1999). Micromorphological observations of feldspar hydrolysis and clay redistribution indicate *in situ* weathering. The tabular carbonates in the lower half of the profile are consistent with calcite precipitation along the vadose–phreatic boundary (Wright and Platt 1995; Alonso-Zarza 2003), suggesting a shallow (< 2 m) water table, which is also supported by ichnological interpretations (see Ichnotaxonomy and Ethological Interpretations section). Lack of redoximorphic features indicates that this pedotype was oxidized and did not experience prolonged water saturation in the Bk1 and Bk2 horizons.

Pedotype I is most similar to modern Aridisols or Inceptisols. The lower Bk horizons have salt pseudomorphs, possibly indicating the presence of a salic horizon. The poor ped structure throughout all profiles examined ($n = 5$) suggests possibly high exchangeable Na^{2+} (Soil Science Division Staff 2017); however, these horizons are not natric because they lack down-profile increases in silicate clay. Stacked calcic and salic horizons also occur in Aridisols; however, reconstructed MAP values are higher than

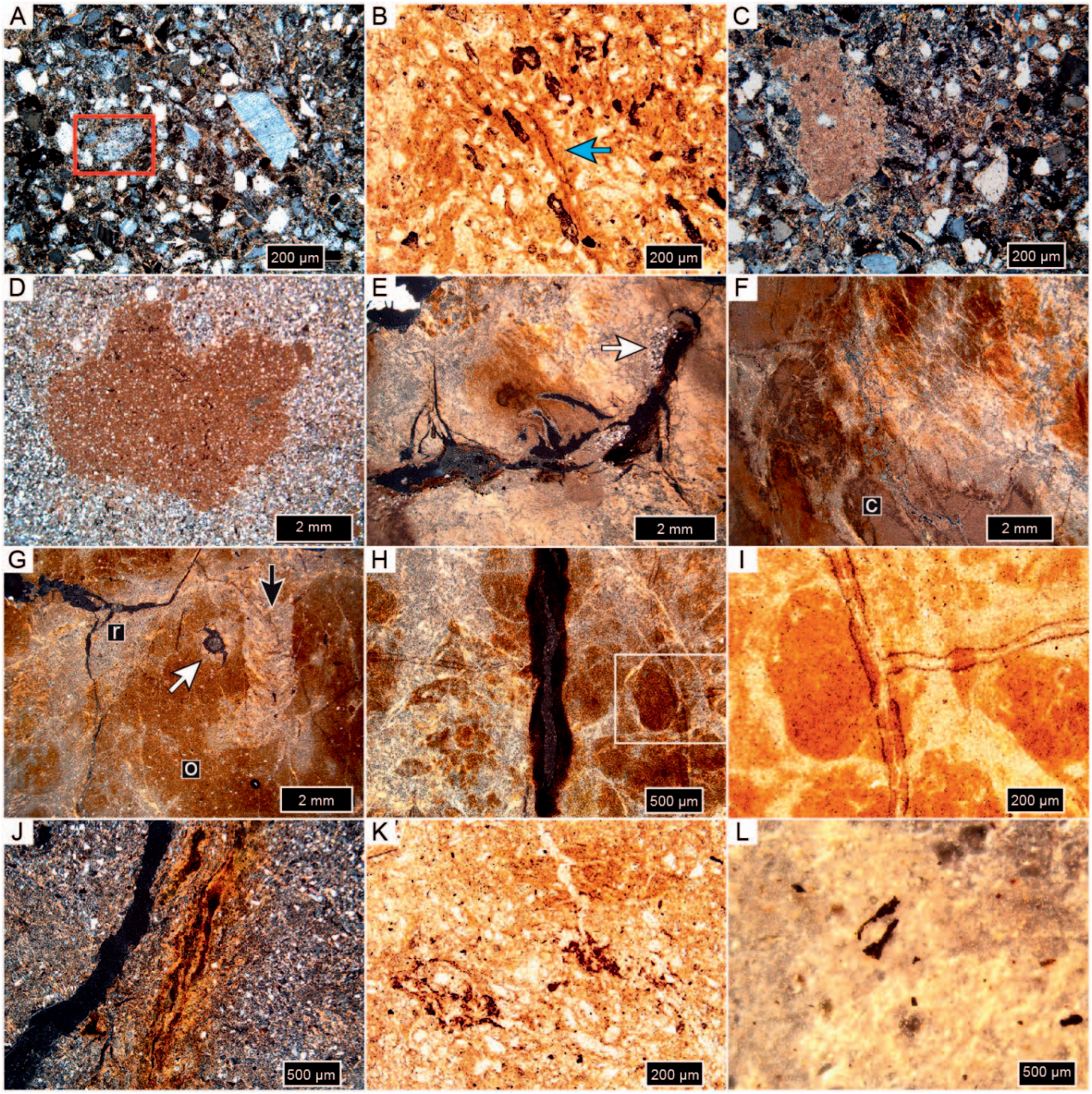

FIG. 8.—Micromorphology of selected paleosol horizons. Cross-polarized light and vertical orientation unless noted. A–D) Bk horizon from Pedotype I. **A)** Weathered (red box) and unweathered feldspars. Note clay coatings on and between grains. **B)** Dark yellow pedogenic clay lining a pore (arrow); plane-polarized light (PPL). **C)** Micritic carbonate nodule with clay coating. **D)** Micritic carbonate mass enveloping detrital silicate grains. E–H) Bkssg horizon of Pedotype VIII. **E)** Fe-Mn root trace with silt infill (arrow). Note clay-rich, Fe-depleted matrix. **F)** Micritic carbonate (c) and well-developed, oriented clay fabric in Fe-depleted matrix. **G)** Oxidized (o) and reduced (r) zones in paleosol matrix, Morphotype II burrow (*Naktodemasis bownii*, black arrow), and cross section of Fe-Mn-lined root trace (white arrow). **H)** Redoximorphic matrix with Fe-Mn root trace and abundant, cross-striated clay fabric. **I)** White box from image H. Ovoid fecal pellet lined with clay, overlain by Fe-Mn-lined root filaments; PPL. J–L) Bg horizon of Pedotype X. **J)** Fe-depleted matrix with clay-filled root trace and striated clay fabric throughout matrix. **K)** Fe-depleted matrix with Fe-Mn masses engulfing detrital silicate grains. PPL. **L)** Fragmented microcharcoal; reflected polarized light.

those in the arid soil-moisture regime (see Paleoclimate Estimations section; Soil Survey Staff 2014).

Pedotype II

Observations of Pedotype II.—Pedotype II (lithofacies Ps) was described at Keefe Canyon Quarry (Fig. 3) and contains an argillic–calcic (Btk) horizon over stacked calcic (Bk and Bkk) horizons. The Btk horizon contains a rubified matrix with clay skins and 2–10% carbonate nodules (Stage II; Gile et al. 1966). Bk horizons have 20–25% carbonate nodules (Stage II), and the laterally discontinuous Bkk horizon is, in places, indurated with 97–100% of the matrix plugged with carbonate (Stage III; Gile et al. 1966). Above and below the Bkk are clay-rich intervals with abrupt boundaries and pedogenic structure. The Keefe Canyon Quarry fauna (Hibbard and Riggs 1949) occurs in the lowermost of these clay-rich intervals (Bk3 horizon). Ped structure is generally poorly developed in all horizons. Parent material is tan fine sand at the top of the profile and brown clay and silt in the lower half of the profile.

Interpretations of Pedotype II.—Pedotype II formed on a succession that transitioned stratigraphically from Fm/Fl mudstones to massive fine sand. This association is similar to Pedotype I and indicates emergence from ponded to subaerial conditions as a result of alluvial and possibly eolian deposition. Pedotype II therefore also formed through cumulization, but with non-steady sedimentation (Kraus 1999). The heterogeneous parent materials were welded via pedogenesis and formed a composite paleosol profile (Kraus 1999). The Bkk horizon occurs at the same stratigraphic level as Lm lithofacies at the Keefe Canyon Turtle section (Fig. 3), and therefore approximates the paleo–water-table position, representing a transition between palustrine facies at Keefe Canyon Turtle to a paleosol at Keefe Canyon Quarry (e.g., Huerta and Armenteros 2005). The presence of the Btk and Bkk horizons indicate that Pedotype II was likely more mature than Pedotype I, as both of these horizon types require very long durations of formation ($\sim 10^3$–10^4 y; Birkeland 1999)

Pedotype II is similar to modern Aridisols and Alfisols. The profile contains an argillic and calcic horizon (Btk) and a petrocalcic horizon (Bkk). Depending on the thickness of material eroded from the paleosol's upper boundary and the soil-moisture regime, it may represent a Paleustalf (Alfisol), or an Agriustoll (Mollisol), but because the surface horizon was not preserved we assign this pedotype to the Alfisol order.

Pedotype III

Observations of Pedotype III.—Pedotype III (lithofacies Ps) has parent material similar to that of Pedotype I but contains a calcareous, gleyed horizon (Bkg) at the base of the profile. The Bkg horizon is generally massive, contains common yellow-orange goethite mottles, and has a low-chroma matrix. Peds have gleyed interiors and oxidized or mottled exteriors. The Bk horizon is oxidized, has prismatic ped structure, and is overlain by the Fm lithofacies (Fig. 7B). Carbonates occur throughout the profile as diffuse matrix impregnations and discrete nodules (2–3 mm wide), consistent with Stage I accumulation (Gile et al. 1966). In the type profile (Raptor Section 2, Fig. 3), the upper boundary is overprinted by carbonate-filled burrows associated with the overlying Fm lithofacies (Fig. 7B).

Interpretations of Pedotype III.—Pedotype III is characterized by an abrupt change in grain size from silt to loamy fine sand that coincides with a marked change in soil hydrology. The boundary between the redoximorphic Bkg horizon and overlying oxidized Bk horizon is lined with carbonate nodules, which demarcates the upper limit of capillary rise and associated carbonate precipitation (Zamanian et al. 2016). The Bkg horizon shows redoximorphic features either due to a higher water-holding capacity (Rawls et al. 1982) or a shallow, fluctuating water table episodically endosaturating the paleosol throughout pedogenesis (Vepraskas 2001). The presence of peds with gleyed interiors and oxidized exteriors is evidence that the paleosol was persistently wet but undersaturated, allowing diffusion of atmospheric O_2 through macrovoids (Wilding and Rehage 1985). Consequently, dissolved Fe^{2+} in ped interiors diffused toward ped boundaries, where it precipitated as Fe^{3+} linings. This can occur as a result of endosaturation (water-table rise) through vertical wicking between grains and does not tend to occur laterally between peds due to the relatively larger space in macrovoids. The silt and loamy fine sand represent different deposits that were welded into a composite paleosol (Kraus 1999).

Pedotype III has subsurface calcic horizons, is endosaturated, and lacks evidence for salic or natric horizons. Based on morphology, this pedotype is most similar to modern Inceptisols.

Pedotype IV

Observations of Pedotype IV.—Pedotype IV (lithofacies Ps) is characterized by a thin solum, with a redoximorphic and calcareous upper horizon (Bkg), overlying an intermittently bedded, fluvial parent material horizon that has similar grain size but lacks redoximorphic features. The generally oxidized matrix of the uppermost horizon (Bkg) contains yellow-orange goethite and hematite masses. Carbonates occur as sparse nodules and thin rhizoliths (Bkg horizon), consistent with Stage I accumulation (Gile et al. 1966).

Interpretations of Pedotype IV.—Although a surface horizon is not preserved, the restriction of redoximorphy to the upper horizon of Pedotype IV and lack of Fe mottling in the lowest horizon indicates variable drainage with possible episaturation (Vepraskas 2001). In Raptor Section 2 (Fig. 3), the paleosol underlies palustrine mud (Fl); thus, episaturation was likely a result of incipient ponding preceding landscape inundation. The thin rhizoliths are consistent with herbaceous vegetation. This paleosol is relatively weakly developed.

Pedotype IV has subsurface calcic horizons, is episaturated, and lacks evidence for salic or natric horizons. Based on morphology, this pedotype is most similar to modern Inceptisols.

Pedotype V

Observations of Pedotype V.—Pedotype V (lithofacies Ps) occurs on red alluvial clayey sand similar to Pedotype IV but lacks pedogenic carbonate. Zones in the matrix are variably oxidized and reduced (Fig. 7C). The Bg horizon contains peds that have oxidized interiors but are coated with mottled and gleyed zones. Yellow-orange goethite and hematite masses are common throughout the Bg horizon. Fe-lined root traces and drab halo root traces are common throughout the profile and tend to be < 0.5 cm wide.

Interpretations of Pedotype V.—Pedotype V occurs in an interval of redoximorphic paleosols and pond deposits in the Keefe Canyon Turtle and Keefe Canyon Quarry sections (Fig. 3). The pedotype is moderately to poorly developed, and the mottling throughout the profiles indicate intermittent water saturation that inhibited soil maturation. The presence of gleying along macrovoids, but with oxidized zones in ped interiors, suggests intermittent episaturation (Vepraskas 2001). This association is the result of downward-percolating water that follows macropores and creates anaerobic conditions between peds. Reduction fronts slowly migrate into the edges of peds; however, if the water drains before peds can become fully depleted of oxygen, then the interior of a ped will remain oxidized and retain its rubified appearance (Vepraskas 2001). The thin root traces indicate herbaceous vegetation cover.

Pedotype V lacks a diagnostic subsurface horizon but shows evidence for episaturation. This pedotype is most similar to Epiaquepts (Inceptisols).

Pedotype VI

Observations of Pedotype VI.—Pedotype VI (lithofacies Pf) formed on fining-upwards alluvial silt and clay, contains a laminated parent material horizon at the base of the profile, and has two stacked argillic (Bt) horizons. Clay skins are common on ped faces, with rare slickensides occurring between angular blocky to wedge peds (Fig. 7D). Reduction mottles are relatively rare and only present in the Bt2 horizon. No carbonates were observed. At the type locality, modern weathering is encroaching on the profile; therefore geochemical and thin-section samples were not collected.

Interpretations of Pedotype VI.—Pedotype VI developed in a single fining-upward, overbank fluvial deposit, representing a stable floodplain surface with simple top-down pedogenesis. The stacked Bt horizons are well developed based on common argillans and well-formed pedogenic structure. The lack of evidence for cummulization indicates that the paleosol formed on a distal, well-drained floodplain (Bown and Kraus 1987; Kraus 1999). Accordingly, Pedotype VI is one of the most mature paleosols in the study area. This pedotype lacks carbonate, thus had circumneutral to acidic soil pH, consistent with the presence of woody vegetation and/or higher rainfall relative to the calcareous pedotypes (e.g., Retallack 2000; Lukens et al. 2018).

Pedotype VI contains stacked argillic horizons, but lacks pedogenic carbonate and is most similar to modern Alfisols.

Pedotype VII

Observations of Pedotype VII.—Pedotype VII (lithofacies Pf) formed on fining-upward, pale-colored alluvial clay and silt. Granular to fine subangular blocky ped structure was observed in the AB horizon. Small carbonate nodules (Stage I; Gile et al. 1966) occur throughout the profile. This pedotype lacks a diagnostic subsurface horizon.

Interpretations of Pedotype VII.—Pedotype VII is a weakly developed paleosol that represents incipient pedogenesis on alluvial parent material. The carbonate nodules throughout the profile are likely an overprint from overlying Pedotype I paleosols. Very thin sediment-filled root traces (1–3 mm) indicate herbaceous vegetation. Incipient alluvial paleosols can form in a large number of environmental conditions, and therefore is only indicative of an unstable landscape position, possibly near a fluvial channel (Bown and Kraus 1987; Retallack 2008).

Pedotype VII lacks significant horizon development and is similar to modern Fluvents (Entisols).

Pedotype VIII

Observations of Pedotype VIII.—Pedotype VIII (lithofacies Pf) contains wedge peds, abundant slickensides, and has a low chroma matrix (Fig. 7E). Yellow-brown goethite and hematite masses and root traces occur throughout the profile. Nodular carbonates (Stage II; Gile et al. 1966) are common in the uppermost horizon (Bkssg).

A thin section from the Bkssg horizon contains an almost exclusively clay matrix, with only rare silt grains that infill root traces (Fig. 8E). The matrix is predominantly reduced with isolated patches of oxidized Fe (Fig. 8F, G). Clay fabric consists of cross-striated matrix impregnations (argillans); granostriated fabric around skeleton grains, carbonates, and fecal pellets; and porostriated fabric along root traces and ped boundaries (Fig. 8G, H). Fe-Mn coatings occur along root filaments, carbonate nodules, and voids. Adhesive meniscate burrows are common, contain clay-lined menisci, and admix reduced and oxidized matrix material (Fig. 8G). Pedogenic carbonate occurs predominantly as micrite with septarian shrinkage cracks (Fig. 8F). Microspar is rare but occurs along shrinkage cracks and along the boundaries of detrital silicate grains in micrite masses. Common hypocoatings occur around root voids and consist of thin filaments of Fe that are separated from root voids by tens of micrometers (Fig. 8H, I). Root traces lined with clay and Fe-Mn are also common in the matrix (Fig. 8E, H).

Interpretations of Pedotype VIII.—Pedotype VIII formed under variable drainage conditions, as represented by the presence of slickensides, redoximorphic features, and carbonate nodules with septarian shrinkage cracks (Beverly et al. 2018). Slickensides specifically indicate the presence of seasonal water saturation and deficit (Nordt et al. 2004). The gleyed ped interiors reflect Fe reduction in the soil matrix due to protracted waterlogged conditions (Soil Science Division Staff 2017). However, coatings of oxidized Fe minerals on ped faces occur throughout the Bkssg horizon, indicating that the paleosol was persistently wet but typically undersaturated, allowing for diffusion of atmospheric O_2 through macrovoids (Wilding and Rehage 1985). Fe hypocoatings on root pores are evidence of redox gradients that formed during root respiration during intermittently water-saturated conditions (Vepraskas 2001). These features indicate that Pedotye VIII formed on a lowland landscape position that was predominantly waterlogged but experienced episodic, possibly seasonal, well drained intervals.

Pedotype VIII is classified as a Vertisol based on the presence of wedge peds, slickensides, and clay texture. The gleyed matrix and calcic suggest the pedotype is similar to modern Calciaquerts.

Pedotype IX

Observations of Pedotype IX.—Pedotype IX (lithofacies Pf) is noncalcareous and formed on fluvio-palustrine clay (lithfacies Fm). The uppermost horizon (Bssg1) is mottled and contains abundant slickensides and wedge peds (Fig. 7F). The Bssg2 horizon is drab with yellow-orange goethite and hematite masses and also contains slickensides. The basal contact of the paleosol is abrupt and sharp on top of a dark gray Fm deposit.

Interpretations of Pedotype IX.—Pedotype IX has predominant vertic features including slickensides and wedge peds, and therefore formed in an environment similar to that of Pedotype VIII (e.g., Nordt et al. 2004). However, in contrast to Pedotype VIII, Pedotype IX lacks carbonate and is strongly mottled with highly variegated coloration due to Fe oxides and hydroxides (Retallack 2008). Pedotype IX is thus interpreted to have formed in a more poorly drained environment than Pedotype VIII, with less common intervals of improved drainage and less evapotranspirative stress. The presence of Fe coated and hypocoated root traces are consistent with hydrophytic vegetation (Bullock et al. 1985). Pedotype IX occurs above the pond or wetland of the Taylor Mollusk bed (Fig. 3), and therefore marks a transition to an emergent, seasonal wetland (Vepraskas 2001).

Pedotype IX is classified as a Vertisol based on the presence of wedge peds, slickensides, and clay texture. The gleyed matrix and evidence of endosaturation are consistent with modern Endoaquerts.

Pedotype X

Observations of Pedotype X.—Pedotype X (lithofacies Pf) lacks slickensides, is characteristically dark in color, and has a Bg horizon with orange Fe-lined root traces along ped boundaries (Fig. 7G). The alluvial parent-material horizon is drab green with primary bedding and carbonized root traces. The matrix is low chroma with green reduction mottles throughout.

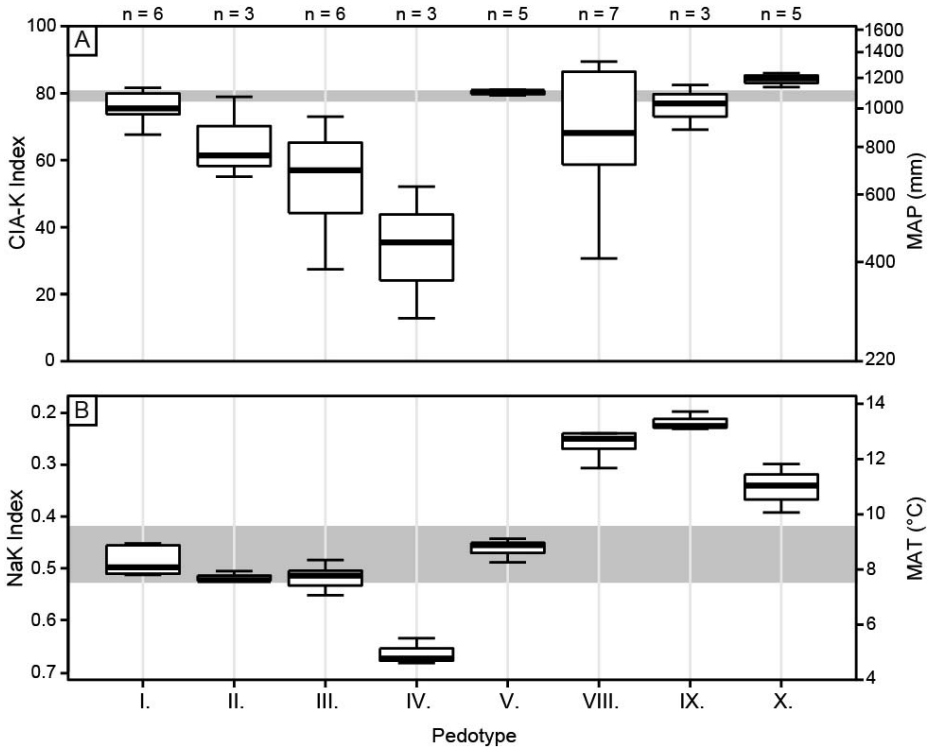

FIG. 9.—Weathering index and corresponding climate estimations for all paleosol B horizon samples, organized by pedotype. Note: the CIA-K transfer function is exponential, causing nonlinear spacing along the secondary y axis in Part A. Gray boxes indicate range of CIA-K values calculated for parent materials, which include alluvial sand, laminated mudstone, and massive clay. MAP, mean annual precipitation; MAT, mean annual temperature.

A thin section from the uppermost horizon (Bg) has a matrix of clay and silt grains. Clays are redistributed as granostriated fabric on detrital grains, porostriated fabric along root voids and ped boundaries, and as rare argillans (Fig. 8J). The matrix is Fe-depleted, as evidenced by pale coloration and rare Fe oxides. Distinct Fe features include coatings on root traces and voids and irregular Fe-Mn masses that engulf silicate grains (Fig. 8K). Microcharcoal fragments are common throughout the matrix (Fig. 8L). Root traces and filaments are abundant. Feldspars occur as both fresh and highly weathered grains. No carbonates were observed.

Interpretations of Pedotype X.—Pedotype X is very poorly drained; however, the lack of slickensides indicates that water deficit was less common than in other poorly drained, fine-grained pedotypes we describe. The presence of illuviated clay and weathered silicate grains indicates *in situ* weathering and necessitates occasional well-drained conditions (Birkeland 1999). The dark drab matrix, presence of Fe coatings and Fe-Mn masses, and carbonized root mats all indicate protracted waterlogging in a wetland (Vepraskas 2001).

Pedotype X is most similar to a Histosol, but the lack of a preserved surface horizon prohibits definitive differentiation between Histosols and other soil orders.

Elemental Geochemistry

The weathering indices, which track various aspects of soil elemental composition, were compared across pedotypes. The CIA-K index can range between 0 and 100, and paleosol B horizon samples from this study span much of this range (Fig. 9A). CIA-K values decrease systematically in pedotypes I–IV (carbonate-bearing, sandy paleosols; Fig. 6). Pedotype V lacks carbonate and has relatively high (~ 80) and invariant CIA-K values. Pedotype VIII has the highest variability in CIA-K values relative to other pedotypes. B horizons from the other two fine-grained pedotypes, however, have well-constrained values between 70 and 85. The elemental composition of fluvial sands and laminated fluvio-palustrine mudstones are used as estimates for paleosol parent materials. CIA-K values for these samples range from 78 to 80.5, with no systematic difference based on grain size. One outlier sample (CIA-K = 63) from a C horizon of Pedotype VIII is not shown in Figure 9A because it likely included a carbonate nodule; the overlying Bkss horizons have CIA-K values of 86–89 and are unlikely to have such an extreme geochemical difference compared to the C horizon, given the weak to moderate pedogenesis. Overall, paleosol B horizons that have higher carbonate content depart from parent-material compositions toward lower CIA-K values, whereas noncalcareous samples are similar to parent-material values.

NaK values range from roughly 0.2 to 0.7 across pedotypes and from 0.42 to 0.55 for parent materials (Fig. 10B). Samples from finer textured soils (Pedotypes VIII-X) tend to have lower NaK values, likely due to lower feldspar abundance in the fine-grained deposits. All silt-size and coarser samples have similar NaK values except Pedotype IV, which has higher NaK values, possibly indicating a slight increase in feldspar content relative to other samples. Salt molds in the lower Bk horizons of Pedotype I are consistent with only moderately high (and not extremely high) NaK values.

Paleoclimate Estimations

Two approaches were taken for reconstructing paleoclimate: 1) transfer functions that relate a weathering index to either MAP or MAT, and 2) the paleosol–paleoclimate model ($PPM_{1.0}$), which co-predicts MAP and MAT using a spline fit on factor scores from a partial least-squares regression analysis (Table 1). In general, estimated values for MAP and MAT are highly variable due to the large range of paleosol types (Fig. 10). For most samples, $PPM_{1.0}$ yields consistently higher MAP values compared to estimations from the CIA-K transfer function (Fig. 10A). This difference has been reported elsewhere (Lukens et al. 2017b) but is poorly understood. Samples that have extremely high MAP predicted by $PPM_{1.0}$ include redoximorphic horizons, which may have accumulated Fe via intermittent mobilization and translocation. This is notable because $PPM_{1.0}$ heavily weights Fe content when modeling MAP (Stinchcomb et

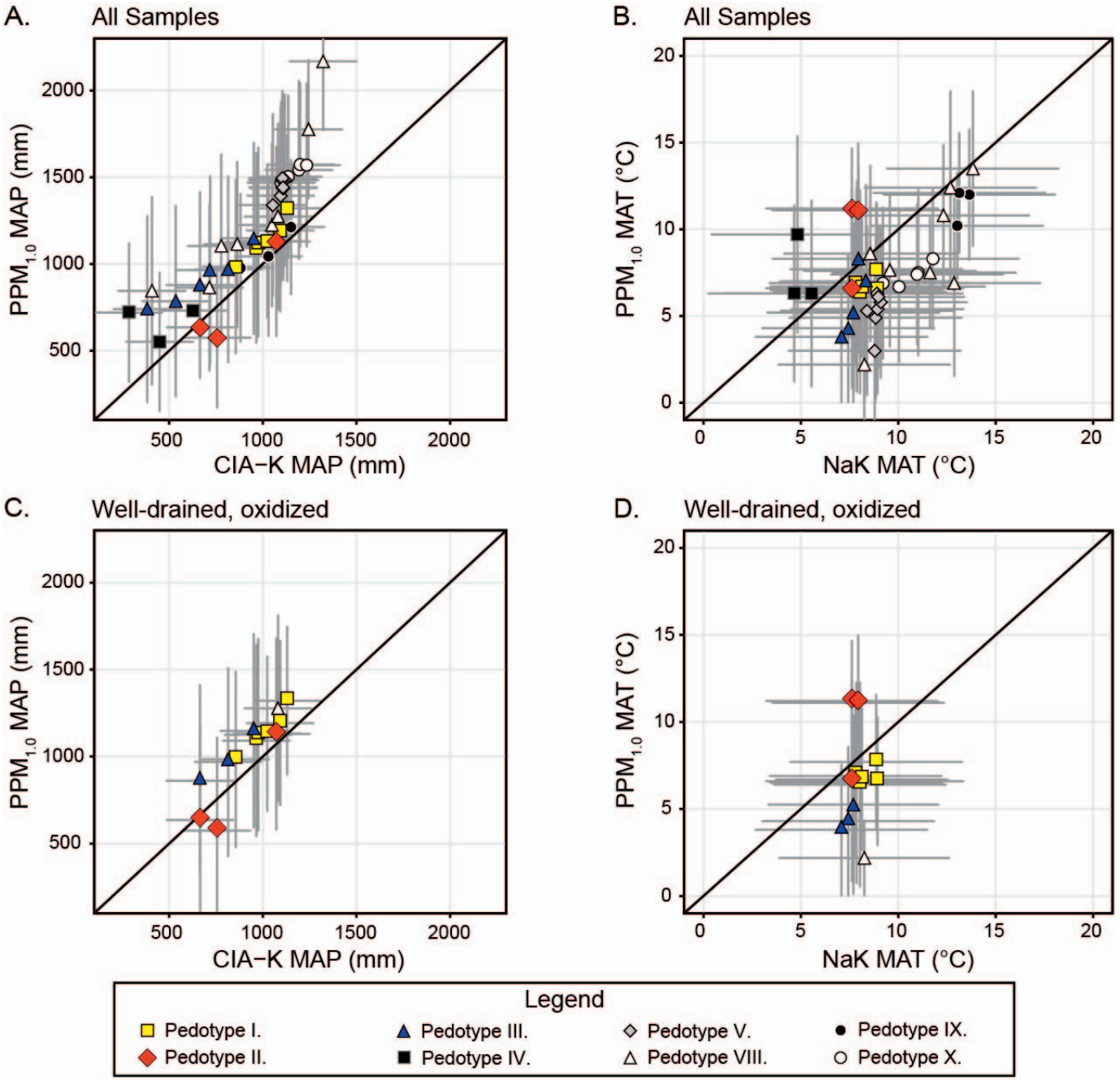

FIG. 10.—Intercomparison of results from the paleosol–paleoclimate model ($PPM_{1.0}$) and traditional transfer functions (CIA-K and NaK). Black lines delineate 1:1 relationship for each plot. Gray bars are model errors. Samples are coded by pedotype. Data in Parts A and B are also shown in Figure 9. **A)** Results from all samples indicate that $PPM_{1.0}$ estimates higher mean annual precipitation (MAP) than CIA-K; values are highly variable. **B)** Results from all samples are highly variable for mean annual temperature (MAT). **C)** MAP results are better constrained and closer to the 1:1 line when only samples from well-drained, oxidized paleosol horizons are included. Estimates range from 500 to 1500 mm. **D)** MAT results are better constrained when only samples from well-drained, oxidized paleosol horizons are included. $PPM_{1.0}$ estimates a larger range compared to the NaK pedotransfer function.

al. 2016). Estimations of MAT are variable across pedotypes and do not show a systematic difference between either of the models used (Fig. 10B).

Paleosols that formed in well drained, oxidizing environments are the most likely to contain geochemical signals that represent the prevailing climate conditions over the time of pedogenesis (Sheldon et al. 2002; Stinchcomb et al. 2016). Paleosol samples from gleyed horizons (chroma $\leq$ 2), redoximorphic horizons, and any horizon with possible phreatic carbonates were filtered from the data set (29 of 41 samples excluded, see Table S2). The culled data set includes 12 uppermost B horizons from Pedotypes I, II, III, and VIII. These paleosol types meet the criteria for application of the CIA-K transfer function (Sheldon et al. 2002), and their range of MAP values (ca. 500–1300 mm) provide the best estimate for the data set overall. These samples show lower variability in the range of MAP values estimated by $PPM_{1.0}$ and CIA-K than the overall data set (Fig. 10C).

TABLE 4.—*Ichnological morphotypes and diagnostic features*.

Morphotype	Morphology	Orientation	Host Matrix	Infill Style and Material	Dimensions	Ichnotaxonomy
I	Unlined, occassional surficial scratches, tunnels branch horizontally in "T" and "Y" junction, knobby and/or hummocky surfaces near junction points of tunnels	Nearly vertical, occassionally transition to subhorizontal and horizontal tunnels	Lm, Fm, Ps lithofacies; Pedotype I	Passive; gray siltstone, micritic carbonate	~ 4–8 cm wide, up to 50 cm long	*Camborygma*
II	Unlined, non-branching, smooth-walled, ellipsoidal packets, meniscate backfill	Random	Ps lithofaces; Pedotype I	Active; indistinct from host matrix	1–2 mm wide, indeterminate length	*Naktodemasis bowni*
III	Unlined, non-branching, smooth-walled, passively filled, simple tubes	Vertical to subvertical and gently curving	Ps lithofaces; Pedotypes I and VII	Passive; infill is finer than host matrix	~ 1–2 cm wide, 10–15 cm long	*Skolithos*
IV	Unlined, smooth-walled, unornamented, straight to sinuous, unbranching	Horizontal, on bedding planes	Fc lithofacies; Pedotype X	Passive; white silt	~ 0.1–0.5 cm wide, indeterminate length	*Planolites*

Whereas the systematically higher MAP estimation associated with $PPM_{1.0}$ is still evident for this subset of samples, values are within error of CIA-K estimations for all samples. Filtering the data set for oxidized and well-drained soils also decreases the range in MAT estimates using the NaK transfer function, but values estimated by $PPM_{1.0}$ are only slightly less variable than the unfiltered data.

ICHNOLOGY

Ichnological Observations

Trace-fossil morphotypes are summarized in Table 4. The most readily recognized ichnofossils (Morphotype I) occur in the Lm, Fm, and Ps lithofacies and are passively filled with either gray siltstone (Fig. 11A–C) or micrite (Fig. 11D, E). Morphotype I is characterized by subvertical shafts with horizontally branching tunnels that have smooth to knobby, hummocky, and/or scratched surfaces (Fig. 11C). These burrows originate in Lm units and occasionally penetrate up to 20–30 cm into underlying Fm or Ps units (Fig. 11E).

Adhesive meniscate burrows (Morphotype II) are abundant in thin sections of Pedotype I (Fig. 8G). These traces are most easily recognized based on the differences in menisci color in comparison to the host matrix. Morphotype II is texturally indistinct from the surrounding media and lacks a preferential orientation.

Morphotype III occurs in the Bk horizons of Pedotype I (Fig. 11F). These tubes are simple in morphology and architecture and are passively filled with sediment that is generally finer relative to the host matrix.

Morphotype IV occurs exclusively in Fc lithofacies. These tunnels are oriented along bedding planes and filled with white silt that contrasts with the dark gray, carbonaceous mudstone matrix (Fig. 11G). Morphotype IV burrows typically do not branch, but do intersect to form what appears to be false branching.

Ichnotaxonomy and Ethological Interpretations

Attributing any of these biogenic structures to a particular organism cannot be definitive because body fossils were not found associated with any observed burrows (Fig. 11). However, given the surficial and architectural morphology, geologic age, and paleoenvironmental context of the traces, some inferences can be made regarding the potential trace makers and their behavior, based on comparison to structures generated by burrowers from analogous, modern settings.

Based on morphology, size, and paleoenvironmental context, Morphotype I traces are assigned to the ichnogenus *Camborygma*, although the size of a trace can be a misleading criterion (Fig. 11A–E; Bedatou et al. 2008; Hasiotis and Mitchell 1993; Hembree 2016). The occasional branches, knobby surfaces, and scratches are consistent with this ichnotaxon (Fig. 11C–E). *Camborygma* are found only in fluvial and lacustrine environments (Hasiotis and Mitchell 1993; Smith et al. 2008; Hembree and Swaninger 2018). Extant freshwater decapod crustaceans, particularly crayfish, construct analogous structures that typically extend to the water table so the lowermost part of the burrow remains flooded (Genise 2016). These dwelling structures protect the aquatic crustaceans from desiccation and predation (Hobbs 1981; Horwitz and Knott 1983; Horwitz et al. 1985; Welch and Eversole 2006; Williner et al. 2014). When the water table drops, the trace maker will extend the depth of the burrow to remain within the phreatic zone (Hasiotis 2007); therefore, the *Camborygma* can be used to infer ancient water-table level and fluctuations (Hasiotis and Dubiel 1993; Hasiotis and Honey 2000; Hasiotis and Mitchell 1993; Hembree and Swaninger 2018). The penetration depth of ~ 50 cm of the *Camborygma* in the Pedotype I profile suggests that the water table during the time of colonization was shallow.

Morphotype II is most similar to *Naktodemasis bowni* (Smith et al. 2008). Laboratory experiments have shown that *N. bowni* are generated as an open, elongate cell that moves through the substrate as the tracemaker removes material from the leading edge of the cell, rotates, and backfills the trailing edge of the cell repeatedly (Smith and Hasiotis 2008; Counts and Hasiotis 2009). A diversity of subterranean insects, such as burrower bugs (Hemiptera: Cydnidae), cicada nymphs (Hemiptera: Cicadidae), and beetle larvae (Coleoptera: Scarabaeidae) generate these structures in modern soils while feeding on roots, xylem sap from roots, and disseminated soil organic matter (White and Strehl 1978; Tashiro 1987). The presence of these backfilled burrows supports the interpretation of subaerial exposure accompanying pedogenesis interpreted for the Pedotype I (Hasiotis 2002; Golab et al. 2018; Wiest et al. 2018).

Morphotype III is classified as *Skolithos* based on the nearly vertical orientation, smooth walls, and structureless fill. The lack of bifurcation or downward tapering is evidence against a root origin. These traces are common across many marine to continental substrates and are therefore not indicative of any specific trace maker.

Morphotype IV is classified as *Planolites* based on the non-branching architecture, lack of ornamentation, and sedimentary infill that is texturally indistinct from the host matrix (Fig. 11G; Pemberton and Frey 1982; Keighley and Pickerill 1995). Extant earthworms generate burrows of

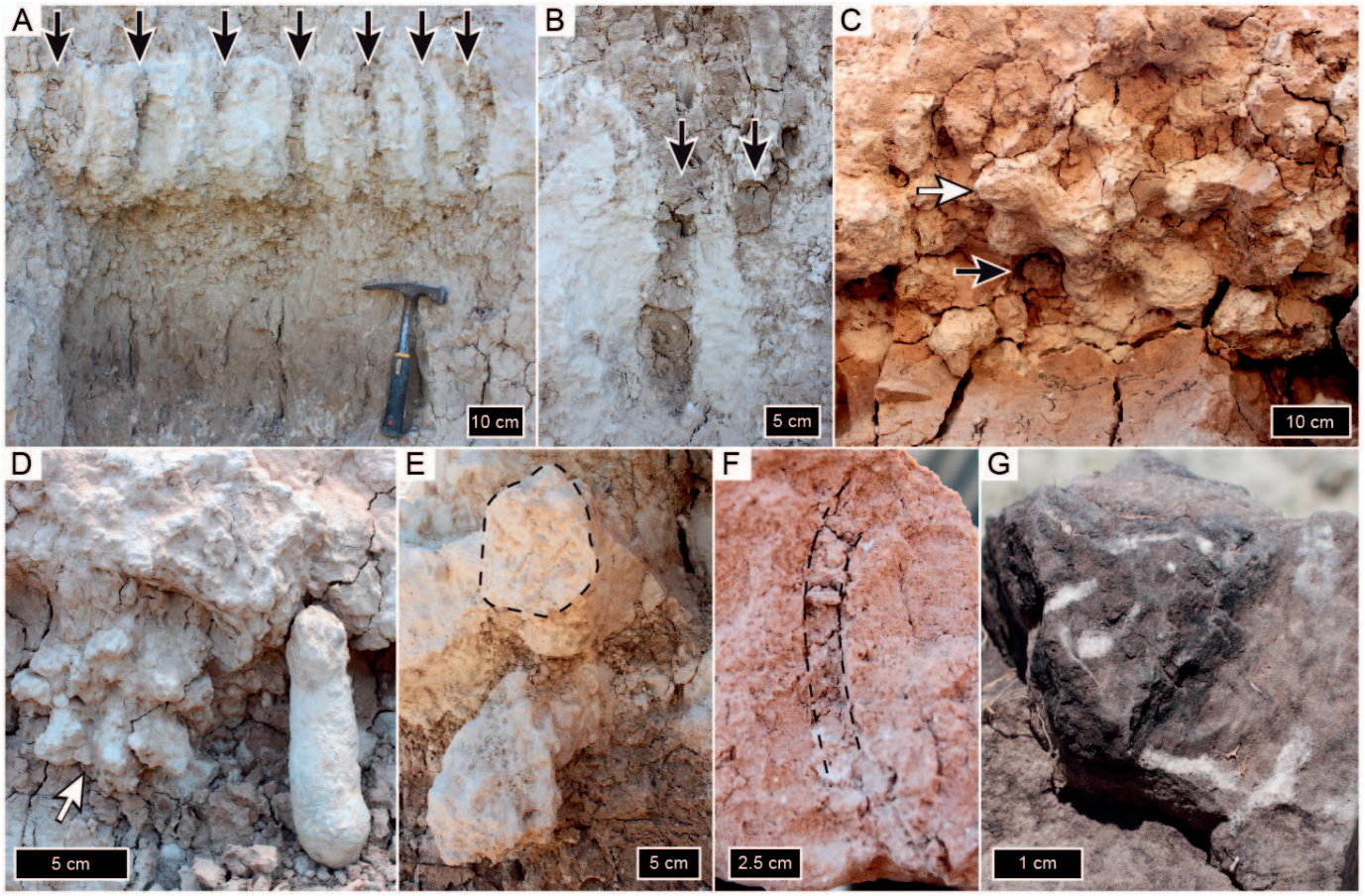

FIG. 11.—Representative trace fossils. **A**, **B)** Morphotype I (arrows) crosscutting Lm lithofacies and filled with gray silt from overlying Fm lithofacies; RP1 outcrop. **C)** Branching and overlapping Morphotype I tunnels with occasional scratch marks (white arrow) along the basal contact of Lm lithofacies, overlying Fm lithofacies. White arrow indicates Lm-filled burrows; black arrow denotes burrow passively filled from an overlying Fm unit; SOTM section. **D)** Branching Morphotype I tunnel with knobby surface texture (white arrow); SOTM section. **E)** Carbonate-filled, subvertical and horizontal tunnels of Morphotype I crosscutting lower boundary of Lm lithofacies; SOTM section. **F)** Morphotype III from Bk horizon of Pedotype I. Burrow is infilled with finer material; SOTM section. **G)** Silt-filled Morphotype IV along bedding plane from Fc lithofacies; XITB section.

comparable size, pattern, and environmental context, and are therefore one possible tracemaker (Lee 1985; Kretzschmar 2004). However, these traces lack fecal pellets, and we note that the relatively simple characteristics of *Planolites* inhibit confident assignment to a specific organism. *Planolites* tracemakers have been documented to tolerate adverse terrestrial conditions associated with wetland environments in other settings (Chin et al. 2013).

DISCUSSION

Facies Model

We propose a facies model for the study interval based on our lithofacies, paleopedological, and ichnological analyses. The model includes fluvial and palustrine end-member environments (Fig. 12), with most of the observed stratigraphic succession recognized as falling between each end member depending on the dominant depositional mode.

Fluvial End Member.—Fluvially dominated depositional phases (Fig. 12A) occur at the base and top of the stratigraphic succession, represented by the Bishop and Wolf gravels. These units are longitudinally traceable for kilometers and represent meandering, bedload-dominated trunk channels based on the variability of current directions at any one locality and the presence of sand dunes with intercalated gravel lag (Fig. 5C–E). A conspicuous difference between the Bishop and Wolf gravels, compared to the smaller, confined channels in the interlaying stratigraphy, is the presence of extrabasinal cobbles and pebbles, indicative of higher competence in the trunk channels bounding the succession. Although much of the floodplain fines associated with these major channels are either not exposed or eroded away (e.g., Fig. 5A), the vertical stacking of oxbow clay plugs (MSL lithofacies, Fig. 4) and presence of alluvial backswamps in the XITB section (shown in breakout section in Fig. 4) indicates that the gravel units were part of large, through-flowing fluvial systems that crosscut the Meade Basin. Paleocurrent directions oriented toward the south-southwest are orthogonal to the modern Cimarron River, but are parallel to the modern Crooked Creek (Fig. 1). Crooked Creek is diverted from the regional drainage pattern due to a north–south-trending normal fault that formed due to recent halotectonically driven subsidence and parallels the axial trend of the basin (Zakrzewski 1975). Subsidence in the Meade Basin during the Pliocene likely deflected the course of the trunk channels from the east–southeast-trending regional drainage pattern.

Backswamps associated with the Bishop Gravel channel are represented by poorly drained paleosols that contain charcoal, hydrophitic vegetation, and lack carbonates (Pedotype X). Oxbow mud plugs (MSL lithofacies) are thick and represent evaporitic, fine-grained ponds or small lakes that were more common and longer-lived on landscapes associated with the Bishop

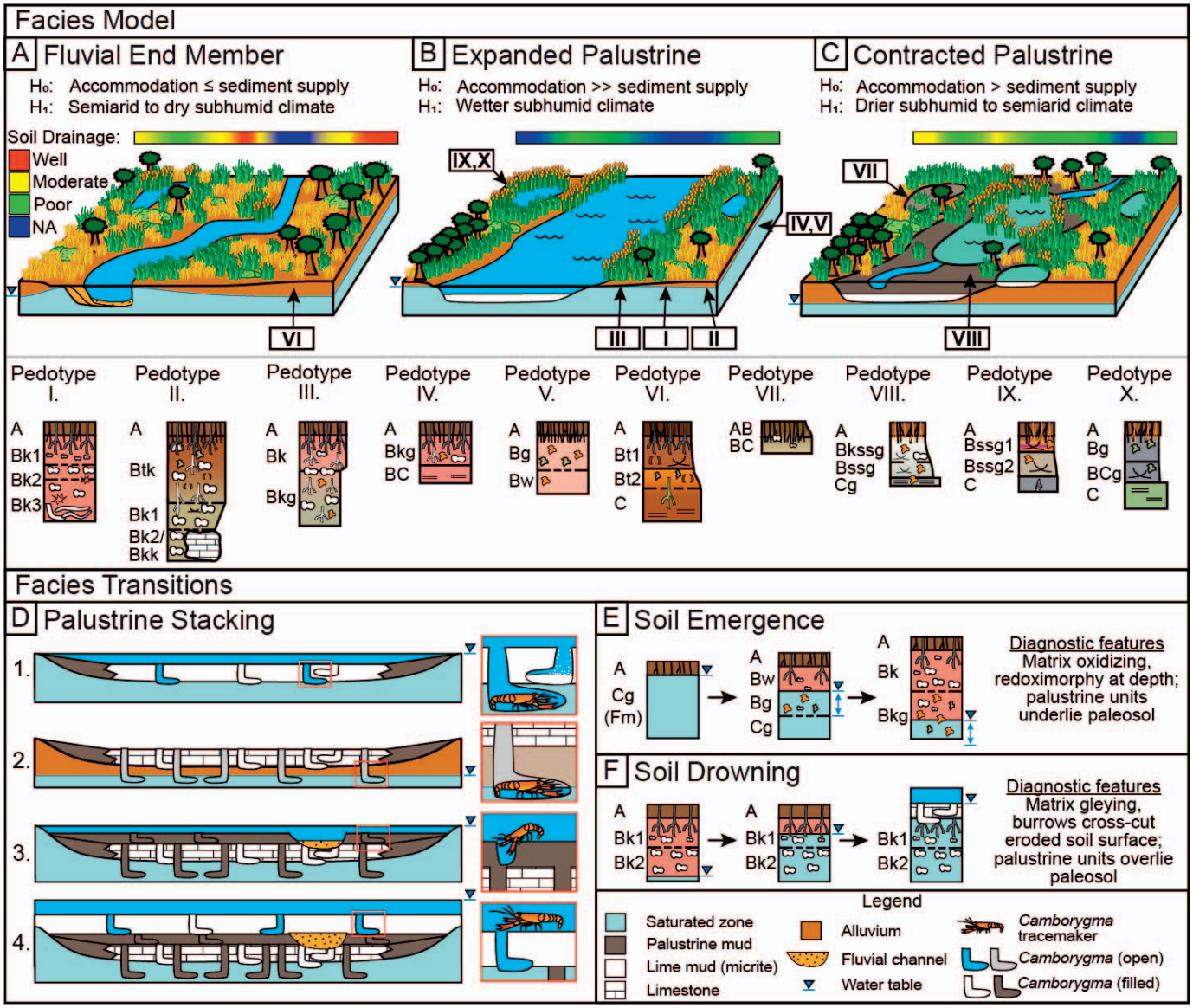

FIG. 12.—Schematic facies model and stratigraphic associations. Null (H_0) and alternative (H_1) hypotheses are given for drivers of each depositional mode. Color bar indicates inferred soil drainage conditions. Landscape positions for each pedotype (roman numerals) is shown. **A)** Fluvially dominated depositional mode, including the Bishop and Wolf Gravel intervals. **B)** Expanded palustrine interval, where evaporative palustrine environments include authigenic carbonate production. **C)** Contracted palustrine interval, where alluvial sedimentation dominates over carbonate formation. Carbonate production is limited to isolated ponds. **D)** Stacking of palustrine facies: 1. Micrite deposition and colonization by *Camborygma* tracemakers during expanded palustrine phase; 2. Water-table drop and deep burrowing by tracemakers; micrite lithifies; 3. Resumption of fluvio-palustrine deposition during palustrine contraction and recolonization; 4. Return to expanded palustrine conditions. **E)** Morphological indicators of soil emergence via aggradational pedogenesis. **F)** Morphological indicators of soil drowning during local base-level rise.

and Wolf Gravel intervals than in the intervening stratigraphy. In general, these observations are consistent with higher-order, meandering river systems draining the southern Rocky Mountains, similar in scale to the modern Cimarron and Canadian rivers (Schumm and Lichty 1963).

Whereas fluvially dominated facies are present at the base and the top of the study interval, much of the stratigraphy between these facies consists of laterally and stratigraphically variable sandy to fine-grained deposits that represent dynamic, aggrading landscapes. Relative to the Bishop and Wolf gravels, the fluvial channels observed in the intervening part of the succession are smaller. Channels tend to be laterally confined and oxbow mudplugs (MSL facies) are rare (e.g., 99-3 Section, Fig. 3). The bases of these channels rarely contain intrabasinal gravel (reworked carbonates and rip-up clasts), and lack the granite, quartzite, and accessory lithic clasts present in the Bishop and Wolf gravels. Taken together, these observations indicate a substantial drop in stream competence after deposition of the Bishop Gravel, signaling a relative increase in accommodation versus sediment supply driven by either local subsidence or climate change (Holbrook and Schumm 1999). Localized subsidence likely decreased stream gradients in the study area, causing an increase in preservation space upstream of geomorphic buttresses (see Fig. 8E in Holbrook et al. 2006). In this model, the net effect on local fluvial geomorphology would be an increase in stream sinuosity and intrabasinal storage of fine-grained sediment.

Palustrine End Member.—The palustrine-dominated interval between the Bishop and Wolf gravels consists of couplets of limestones (Lm) and mudstones (Fm, Fl) interbedded with paleosols or small fluvial channels. These facies represent two alternating depositional modes (Fig. 12B, C). The first consists of expanded palustrine phases marked by laterally extensive micritic limestones (e.g., CC1, Fig. 3) that crosscut and impregnate preexisting deposits, including fluvial channels (Fig. 5H), and are traceable to phreatically influenced calcareous paleosols (Pedotype II, Fig. 3).

A contracted palustrine depositional mode is also evident, which is dominated by siliciclastic sedimentation with localized precipitation of nodular to diffuse, non-pedogenic carbonate in subaqueous mud (Fig. 12C). The Fm and Fl lithofacies define this depositional phase and contain gastropods in mudstones that lack pedogenic structure or root traces. These facies represent wetland margins and/or shallow ponds that received fluvial sedimentation from single-story, through-flowing streams (Fig. 5H). During the contracted palustrine phases, deposition of fine-grained siliciclastic alluvium is predominant and carbonate production is restricted to isolated, evaporative ponds. Whereas palustrine expansion results in lateral connectivity of Lm lithofacies, contracted palustrine settings are characterized by Lm units that pinch out laterally between small fluvial channels and siliciclastic mudstones (Fm/Fl).

Facies Transitions.—Stratigraphic stacking of depositional styles is evident in the tiering of *Camborygma* (Morphotype I) in Lm and Fm/Fl lithofacies (Fig. 12D). The Lm lithofacies commonly contains micrite-filled *Camborygma* (Fig. 9C–E). Because crayfish do not burrow through consolidated substrates, the passively filled burrows indicate subaqueous excavation, occupation, and abandonment of domiciles contemporaneous with unconsolidated micrite deposition (Fig. 12D, event 1; Hasiotis et al. 2012). The Lm lithofacies is commonly overlain by massive siltstone (Fm) and typically includes silt-filled *Camborygma* that crosscut the limestone (Fig. 9A, B). These traces suggest that, when Lm units were subaerially exposed during contracted palustrine conditions, crayfish burrowed to the water table before the limestone consolidation (Fig. 12D, event 2). The *Camborygma* were passively filled with gray silt after siliciclastic sedimentation resumed (Fig. 12D, event 3). In some cases, the depositional mode returned to carbonate-dominated, expanded palustrine conditions (e.g., SOTM section, Fig. 3; Fig. 12D, event 4). The commonly occurring Lm-Fm facies association represents a depositional succession shifting from clear and calm, evaporative shallow lakes during palustrine expansion to brief intervals of subaerial exposure, and then to interconnected ponds that received clastic input from through-flowing streams during palustrine contraction.

The brief intervals of subaerial exposure that are required to consolidate Lm units before siliciclastic deposition are conspicuously not associated with weathering. Extensive desiccation and reworking of palustrine limestones have been observed in other systems and is attributed to pedogenic modification and fluvial reworking (Wright and Platt 1995; Alonso-Zarza and Calvo 2000; Tanner 2000; Alonso-Zarza et al. 2011). The absence of these features in any of the observed stratigraphic sections indicates that Lm units were exposed for brief intervals of time, likely less than one year (Alonso-Zarza and Calvo 2000).

Depositional units transition laterally from subaqueous to subaerial over hundreds of meters in any one canyon, indicating that while paleotopographic variations were present, they were subtle and water depth was never more than $\sim$ 1–2 m deep. The combination of pedogenic drainage features and facies juxtaposition allows for reconstruction of time-transgressive changes in water-table position. Paleosols that evince gradual emergence are underlain by palustrine deposits and have endosaturated features in the lower parts of their profiles (Fig. 12E). For example, unit 2 in the RP2 section is a Pedotype II paleosol directly overlying palustrine siltstone (Fm). Endosaturation in this pedotype is characterized by gleying and mottling in the basal Bkg horizon. Similarly, Pedotype I paleosols in Fox Canyon occur above palustrine siltstones (Fm) and limestones (Lm) and contain carbonate ribbons, tabular calcretes, and salt pseudomorphs in the lowest Bk horizons. These features suggest that sedimentation gradually elevated the land surface above the reach of a fluctuating water table, likely as fluvial sedimentation resumed during a phase of palustrine contraction (Fig. 12E).

Gradual inundation of landscapes also occurred and is represented by paleosols with morphologies indicative of episaturated conditions, which are both lateral to and overlain by Lm lithofacies (Fig. 12F). These include the occurrence of the Pedotypes I, III, and IV in the Raptor sections (RP1 and RP2). Each paleosol underlies either Lm or Fm/Fl units, have gleyed zones in the upper 10–20 cm of each profile, and *Camborygma* burrows overprint the uppermost horizon in each profile (e.g., Fig. 6B). Expansion of palustrine units above subaerially exposed paleosols caused erosion of soil surfaces, resulting in truncated profiles without A horizons.

Paleolandscape Positions.—The Meade Basin pedotypes represent differing combinations of soil-forming state factors (Eq. 1) and, as such, the paleosols preserve environmental information on geomorphic positions and processes (Fig. 12A–C). Pedotypes I, II, and III all have similar silty to sandy alluvial parent material, herbaceous root traces ($<$ 5 mm wide), and are highly calcareous. These paleosols are transitional between endo-saturated to well-drained conditions. Pedotype III is endosaturated, and likely formed near lake margins during the expanded palustrine interval. Pedotypes I and II are better drained, but because both formed in communication with the water table, they must have developed on higher landscape positions upslope from Pedotype III.

Pedotype IV and V are episaturated and likely formed during the expanded palustrine phase near perched water tables or seasonally flooded ponds on alluvial terraces. Similarly, Pedotypes VIII, IX, and X would have formed in fine-grained deposits associated with wetlands or ponds in palustrine phases, but with variable durations of subaerial exposure. Slickensides in these vertic paleosol types indicate substantial contrasts in drainage conditions annually and suggests that the depth and extent of wetlands and ponds were highly variable.

Pedotype VII could have formed on briefly exposed siliciclastic sediments during any depositional phase. In contrast, Pedotype VI is indicative of the most well developed paleosols. The lack of carbonate and moderate root-trace diameters suggests that Pedotype VI formed in shrubland to open forests. The rarity of Pedotype VI in the study interval indicates either that a preservation bias existed for lowland landscapes, or that shrubland to open forest biomes were relatively rare at this time, which is consistent with the fossil rodent assemblages.

Controls on Landscape Evolution

In general, the stratigraphy described in this study is flat-lying and lacks evidence of extensive warping, tilting, or deformation where examined in the field. Crevasses have been observed in localized zones and occasionally contain vertebrate fossils (Hibbard and Riggs 1949). There is only slight folding in the outcrops at Keefe Canyon, notably at the 99-3 outcrop. Accommodation generated by subsurface evaporite dissolution was likely widespread and gradual, and did not generally result in extensive, localized deformation observed in other halotectonic settings, such as southern Utah (Prochnow et al. 2006), although exceptions are evident in some outcrops in the Meade Basin.

Disentangling the influences of subsidence and climate on fluctuations in the water table throughout the study interval is difficult. Results from paleosol analyses indicate that climate was likely subhumid, which agrees with climate regimes suitable for palustrine facies in modern systems (Alonso-Zarza 2003) and is also consistent with the fossil rodent assemblages. Without more precise control on the age of strata and the

climate patterns of the midcontinent during the Pliocene, we posit a null hypothesis that drainage was controlled principally by tectonic and geomorphic factors, particularly the balance between subsidence and sediment supply. Intervals with accommodation less than or equal to sediment supply would have been dominated by the fluvial end-member facies, whereas accommodation gain greatly outpacing sediment supply would result in the expansion of palustrine environments (Fig. 12A–C). Studies of dissolution-induced subsidence in the Ebro Basin of NE Spain show that increased subsidence rates resulted in a change in channel pattern from braided to meandering, increased deposition of fine-grained overbank facies, and the appearance of palustrine environments in the subsidence affected area (Benito et al. 2000; Guerrero et al. 2008). These observations are in line with the geomorphic transition from large, bedload-dominated channels with gravel lags (Bishop Gravel) to suspended-load-dominated streams with smaller dimensions in the middle of the stratigraphic succession. The Wolf Gravel, in the upper part of the succession, marks a return to high-gradient, bedload channels, suggesting either a decrease in subsidence rates or an increase in sediment supply to the basin (Holbrook and Schumm 1999; Holbrook et al. 2006). Sediment supply may have increased due to increased gradients upstream of the area of subsidence and the resultant migration of knickpoints through the fluvial system (Schumm 1993, Layzell et al. 2015).

We also propose an alternative hypothesis, where the El Niño–like state of the Pliocene equatorial Pacific Ocean (Ravelo et al. 2006) could have led to climatic control on the water table position and ponding in the Meade Basin. This climate state, termed El Padre (Ravelo et al. 2014), resembles the sea-surface-temperature pattern of an El Niño event but is a perennial, long-lived climate state in contrast to the dynamic, quasi-periodic, sub-decadal El Niño Southern Oscillation between El Niño and La Niña states. Some studies indicate that rainfall patterns associated with El Padre would increase precipitation amounts in the Meade Basin region (e.g., Goldner et al. 2011). In this scenario, the fine-grained, palustrine-dominated interval between the Bishop and Wolf gravels is the result of increased rainfall associated with El Padre rather than tectonic subsidence. While we have no direct support for this mechanism at present, we cannot rule out a climatic driver for the facies changes observed in the Meade Basin succession.

Vertebrate fossil localities in Keefe Canyon tend to occur along the surfaces of palustrine mudstones, suggesting that desiccating-watering-hole scenarios may have been a cause of death for large mammals (Honey et al. 2005). For example, Keefe Canyon Quarry fauna (see Fig. 3) is preserved immediately above a thin mudstone (Fm) unit that was deposited in standing water. Hibbard and Riggs (1949) interpreted the assemblage to represent a congregation around a spring or standing water. Immediately above the massive mudstone is a highly calcareous, well drained, and very mature paleosol (Pedotype II). Similarly, the proposed mechanism for palustrine limestone formation requires intermittent desiccation of ponded water (Fig. 12D), indicating that drought or other major changes in drainage may have been a key stressor on the local faunal community.

In general, the presence of palustrine siltstone and limestone units and hydromorphic paleosols throughout the succession indicate that standing water was frequently present on paleolandscapes. To first order, this supports using the CC1 horizon as a correlative stratigraphic unit, regardless of the fact that carbonate morphology varies laterally in the horizon. At the Raptor outcrop, CC1 consists of carbonate cement along trough cross-beds in a fluvial channel (Fig. 5H). At the same elevation in the adjacent 99-3 outcrop and the Keefe Canyon Turtle outcrop, CC1 occurs as the Lm lithofacies with common *Camborygma* isp. At Keefe Canyon Quarry, the CC1 layer occurs as an intermittent Bkk horizon at the base of the Pedotype II paleosol.

These laterally persistent carbonates that crosscut facies transitions are evidence that inundation of heterogeneous landscapes occurred by an external mechanism—namely subsidence and groundwater discharge—which submerged both channels and overbank facies in alkaline water. The carbonate cements that follow cross-beds in the Raptor outcrop are likely due to overprinting by palustrine carbonates. This also suggests that the Bkk horizon of Pedotype II at Keefe Canyon Quarry was overthickened via phreatic influence, possibly on the margin of an alkaline lake. The lateral correlation of CC1 across Keefe Canyon indicates that the lake was at least ca. 500 m wide. Honey et al. (2005) laterally traced lithologic contacts across the canyons north of the Cimarron River, and correlated CC1 with carbonate units in Fox Canyon. We observed that multiple palustrine Lm units and pedogenic carbonate horizons occur in all canyons, so we cannot be certain that any one carbonate unit corresponds to the same "CC1" bed that occurs in Keefe Canyon. If the limestones are indeed laterally correlative between the canyons, then the observable width of any one paleolake would have been on the order of 2,000 m. Most Lm units are tiered throughout the stratigraphy and laterally pinch out and were therefore part of many smaller lakes that existed diachronously.

Over 30,000 modern playas have been documented in the Great Plains. These are small ($<$ 1 km wide) depressions that become filled with lacustrine mud and carbonate, and eolian sand and silt, and occasionally have Vertisols weathered into exposed smectitic mud fills (Osterkamp and Wood 1987; Wood and Osterkamp 1987; Holliday et al. 1996). Holliday et al. (1996) conclude that fluvial erosion and deflationary processes are the primary agents that develop modern playas, rather than dissolution of underlying calcretes or limestone bedrock. The palustrine deposits documented in this study are similar in size to these playas but differ in their origin and infilling material—carbonates are thicker and more abundant in the Meade Basin sections, and we have yet to unequivocally document eolian sediments. Unlike palustrine carbonates documented from other low-relief settings, we found no evidence of stromatolites, peloids, ooids, or surficial karstification (Wright and Platt 1995; Tanner 2000; Melchor et al. 2002). The carbonate units we observed were dominantly micritic and massive with flat upper contacts and lack evidence of pedogenic modification. The Meade Basin palustrine facies were therefore unique relative to modern systems in the region, and represent a different combination of tectonics, climate, and/or other possible agents of landscape development.

CONCLUSIONS

The depositional environments of the Meade Basin were highly dynamic in the early to middle Pliocene, marked by halotectonically driven subsidence and possibly influenced by an enhanced ENSO-affected climate state. Shifts from subaqueous to subaerial facies were both gradual and rapid, and were differentially expressed along paleocatenas. Fluctuating groundwater levels affected the distribution of palustrine and pedogenic carbonates and likely caused overprinting between morphological associations. Ongoing petrographic and stable-isotope analysis of individual carbonate phases should help to disentangle vadose, phreatic, and diagenetic influences on carbonate formation. Several hypotheses proposed in this study will be addressed in future studies, including testing the role of climate on intrabasinal flooding events and testing the association between pedotypes and inferred vegetation cover. Though noisy, the climate signals preserved in the Pliocene record of the Meade Basin indicate that the western Great Plains were possibly wetter in a climate state potentially analogous to future warming scenarios.

ACKNOWLEDGMENTS

We are thankful to the many field assistants who facilitated data collection over several summers, including, K. Chambers, M. Haralson, T. Hoffman, K. Jackson, R. McCreesh, and H. Richardson. This work was improved through conversations in the field with J. Gosse, G. Ludvigson, J. Smith, and C. Strömberg. We are also grateful to landowners in and around Meade, Kansas, for access to field sites. Funding for this work was provided by Baylor

Geoscience Department Graduate Research Grants to W.E.L., the Kansas Geological Survey, the U.S. National Science Foundation Sedimentary Geology Program to D.L.F. (EAR-0207383), and R.A.M. (EAR-0207582) and from the Earth-Life Transitions program to D.L.F. (EAR-1338262), K.F-D. (EAR-1338313), K.E.S. (and J. Eiler; EAR-1338261), P.J.P., and K.T.U. (EAR-1338243), and from the National Geographic Society to R.A.M. (5963-07, 6547-99) with matching funds to R.A.M. from Murray State University. We thank associate editor P.J. McCarthy, V.P. Wright, and an anonymous reviewer for comments that greatly improved this manuscript. Our work in the Meade Basin relies heavily on the insights of our late friend and colleague Jim Honey, whose years of field work in the area provided broad and strong shoulders for us to stand on today. We miss him greatly.

SUPPLEMENTAL MATERIAL

Supplemental Tables S1 and S2 are available from JSR's Data Archive.

REFERENCES

Allmendinger, R.W., 2018, Stereonet, v. 10.0.

Alonso-Zarza, A.M., 2003, Palaeoenvironmental significance of palustrine carbonates and calcretes in the geological record: Earth-Science Reviews, v. 60, p. 261–298.

Alonso-Zarza, A.M., and Calvo, J.P., 2000, Palustrine sedimentation in an episodically subsiding basin: the Miocene of the northern Teruel Graben (Spain): Palaeogeography, Palaeoclimatology, Palaeoecology, v. 160, p. 1–21.

Alonso-Zarza, A.M., Genise, J.F., and Verde, M., 2011, Sedimentology, diagenesis and ichnology of Cretaceous and Palaeogene calcretes and palustrine carbonates from Uruguay: Sedimentary Geology, v. 236, p. 45–61.

Bedatou, E., Melchor, R.N., Bellosi, E., and Genise, J.F., 2008, Crayfish burrows from Late Jurassic–Late Cretaceous continental deposits of Patagonia, Argentina: their palaeoecological, palaeoclimatic and palaeobiogeographical significance: Palaeogeography, Palaeoclimatology, Palaeoecology, v. 257, p. 169–184.

Bell, C.J., Lundelius, E.L., Jr., Barnosky, A.D., Graham, R.W., Lindsay, E.H., Ruez, D.R., Jr., Semken, H.A., Jr., Webb, S.D., and Zakrewski, R.J., 2002, The Blancan, Irvingtonian, and Ranchlabrean Mammal Ages, *in* Woodburne, M.O., ed., Late Cretaceous and Cenozoic Mammals of North America: Biostratigraphy and Geochronology: New York, Columbia University Press, p. 232–314.

Benito, G., Gutiérrez, F., Pérez-González, A., and Machado, M.J., 2000, Geomorphological and sedimentological features in Quaternary fluvial systems affected by solution-induced subsidence (Ebro Basin, NE-Spain): Geomorphology, v. 33, p. 209–224.

Beverly, E.J., Lukens, W.E., and Stinchcomb, G.E., 2018, Paleopedology as a tool for reconstructing paleoenvironments and paleoecology, *in* Croft, D.A., Su, D.F., and Simpson, S.W., eds., Methods in Paleoecology: Reconstructing Cenozoic Terrestrial Environments and Ecological Communities: Switzerland, Springer, p. 151–183.

Birkeland, P.W., 1999, Soils and Geomorphology, Third Edition: Oxford, U.K., Oxford University Press, 430 p.

Bown, T.M., and Kraus, M.J., 1987, Integration of channel and floodplain suites, I. Developmental sequence and lateral relations of alluvial paleosols: Journal of Sedimentary Petrology, v. 57, p. 587–601.

Brewer, R., 1964, Fabric and Mineral Analysis of Soils: New York, Wiley, 73 p.

Bridge, J.S., 2003, Rivers and Floodplains: London, Blackwell, 491 p.

Bullock, P., Fedoroff, N., Jungerius, A., Stoops, G., and Tursina, T., 1985, Handbook of Soil Thin Section Description: Albrighton, UK, Waine Research Publications, 152 p.

Chin, K., Pearson, D., and Ekdale, A.A., 2013, Fossil worm burrows reveal very early terrestrial animal activity and shed light on trophic resources after the end-Cretaceous mass extinction: PLoS One, v. 8, e70920.

Counts, J.W., and Hasiotis, S.T., 2009, Neoichnological experiments with masked chafer beetles (Coleoptera: Scarabaeidae): implications for backfilled continental trace fossils: Palaios, v. 24, p. 74–91.

De Schepper, S., Schreck, M., Beck, K.M., Matthiessen, J., Fahl, K., and Mangerud, G., 2015, Early Pliocene onset of modern Nordic Seas circulation related to ocean gateway changes: Nature Communications, v. 6, no. 8659.

Eaton, G.P., 2008, Epeirogeny in the Southern Rocky Mountains region: evidence and origin: Geosphere, v. 4, p. 764–784.

Fisher, N.I., Lewis, T., and Embleton, B.J., 1987, Statistical Analysis of Spherical Data: Cambridge, U.K., Cambridge University Press, 329 p.

Fisher, R., 1953, Dispersion on a sphere: Royal Society of London, Series A, Mathematical, Physical and Engineering Sciences, Proceedings, v. 217, p. 295–305.

Fox, D.L., and Koch, P.L., 2003, Tertiary history of C_4 biomass in the Great Plains, USA: Geology, v. 31, p. 809–812.

Fox, D.L., Honey, J.G., Martin, R.A., and Peláez-Campomanes, P., 2012a, Pedogenic carbonate stable isotope record of environmental change during the Neogene in the southern Great Plains, southwest Kansas, USA: carbon isotopes and the evolution of C_4-dominated grasslands: Geological Society of America, Bulletin, v. 124, p. 444–462.

Fox, D.L., Honey, J.G., Martin, R.A., and Peláez-Campomanes, P., 2012b, Pedogenic carbonate stable isotope record of environmental change during the Neogene in the southern Great Plains, southwest Kansas, USA: oxygen isotopes and paleoclimate during the evolution of C_4-dominated grasslands: Geological Society of America, Bulletin, v. 124, p. 431–443.

Franks, P.J., Royer, D.L., Beerling, D.J., Van de Water, P.K., Cantrill, D.J., Barbour, M.M., and Berry, J.A., 2014, New constraints on atmospheric CO_2 concentration for the Phanerozoic: new constraints on Phanerozoic CO_2: Geophysical Research Letters, v. 41, p. 4685–4694.

Frye, J.C., and Schoff, S.L., 1942, Deep-seated solution in the Meade basin and vicinity, Kansas and Oklahoma: American Geophysical Union, EOS, Transactions, v. 23, p. 35–39.

Genise, J.F., 2016, Ichnoentomology: Insect Traces in Soils and Paleosols: Switzerland, Springer, 695 p.

Gierlowski-Kordesch, E., Finkelstein, D.B., Truchan Holland, J.J., and Kallini, K.D., 2013, Carbonate lake deposits associated with distal siliciclastic perennial-river systems: Journal of Sedimentary Research, v. 83, p. 1114–1129.

Gile, L.H., Peterson, F.F., and Grossman, R.B., 1966, Morphological and genetic sequences of carbonate accumulation in desert soils: Soil Science, v. 101, p. 347–360.

Golab, J.A., Smith, J.J., and Hasiotis, S.T., 2018, Paleoenvironmental and paleogeographic implications of paleosols and ichnofossils in the Upper Pennsylvanian Halgaito Formation, southeastern Utah: Palaios, v. 33, p. 296–311.

Goldner, A., Huber, M., Diffenbaugh, N., and Caballero, R., 2011, Implications of the permanent El Niño teleconnection "Blueprint" for past global and North American hydroclimatology: Climate of the Past, v. 7, p. 723–743.

Goodwin, H.T., and Martin, R.A., 2017, Ground squirrels (Rodentia, Sciuridae) of the late Cenozoic Meade Basin sequence: diversity and paleoecological implications: Journal of Paleontology, v. 91, p. 1244–1257.

Guerrero, J., Gutiérrez, F., and Lucha, P., 2008, Impact of halite dissolution subsidence on Quaternary fluvial terrace development: case study of the Huerva River, Ebro Basin, NE Spain: Geomorphology, v. 100, p. 164–179.

Gustavson, T.C., 1986, Geomorphic development of the Canadian River Valley, Texas Panhandle: an example of regional salt dissolution and subsidence: Geological Society of America, Bulletin, v. 97, p. 459–472.

Hasiotis, S.T., 2002, Continental Trace Fossils: SEPM, Short Course Notes 51, 132 p.

Hasiotis, S.T., 2007, Continental ichnology: fundamental processes and controls on trace fossil distribution: Trace Fossils, Elsevier, p. 268–284.

Hasiotis, S.T., and Dubiel, R.F., 1993, Crayfish burrows and their paleohydrologic significance: Upper Triassic Chinle Formation, Ft. Wingate, New Mexico: New Mexico Museum of Natural History and Science, Bulletin, v. 3, p. 24–26.

Hasiotis, S.T., and Honey, J., 2000, Paleocene continental deposits and crayfish burrows of the Laramide basins in the Rocky Mountains: paleohydrologic and stratigraphic significance: Journal of Sedimentary Research, v. 70, p. 127–139.

Hasiotis, S.T., and Mitchell, C.E., 1993, A comparison of crayfish burrow morphologies: Triassic and Holocene fossil, paleo- and neo-ichnological evidence, and the identification of their burrowing signatures: Ichnos, v. 2, p. 291–314.

Hasiotis, S.T., Platt, B.F., Reilly, M., Amos, K., Lang, S., Kennedy, D., Todd, J.A., and Michel, E., 2012, Actualistic studies of the spatial and temporal distribution of terrestrial and aquatic organism traces in continental environments to differentiate lacustrine from fluvial, eolian, and marine deposits in the geologic record, *in* Baganz, O.W., Bartov, Y., Bohacs, K., and Nummedal, D., eds., Lacustrine Sandstone Reservoirs and Hydrocarbon Systems: American Association of Petroleum Geologists, Memoir 95, p. 433–489.

Hembree, D., 2016, Using experimental neoichnology and quantitative analyses to improve the interpretation of continental trace fossils: Ichnos, v. 23, p. 262–297.

Hembree, D.I., and Swaninger, E.S., 2018, Large *Camborygma* isp. in fluvial deposits of the Lower Permian (Asselian) Dunkard Group, southeastern Ohio, USA: Palaeogeography, Palaeoclimatology, Palaeoecology, v. 491, p. 137–151.

Hibbard, C.W., 1950, Mammals of the Rexroad Formation from Fox Canyon, Kansas: Contributions from the Museum of Paleontology, University of Michigan, v. 8, p. 113–192.

Hibbard, C.W., and Riggs, E.S., 1949, Upper Pliocene vertebrates from Keefe Canyon, Meade County, Kansas: Geological Society of America, Bulletin, v. 60, p. 829–860.

Hibbard, C.W., and Zakrzewski, R.J., 1972, A new species of microtine from the late Pliocene of Kansas: Journal of Mammalogy, v. 53, p. 834–839.

Hobbs, H.H., Jr., 1981, The Crayfishes of Georgia: Smithsonian Contributions to Zoology, no. 166, 549 p.

Holbrook, J., and Schumm, S.A., 1999, Geomorphic and sedimentary response of rivers to tectonic deformation: a brief review and critique of a tool for recognizing subtle epeirogenic deformation in modern and ancient settings: Tectonophysics, v. 305, p. 287–306.

Holbrook, J., Scott, R.W., and Oboh-Ikuenobe, F.E., 2006, Base-level buffers and buttresses: a model for upstream versus downstream control on fluvial geometry and architecture within sequences: Journal of Sedimentary Research, v. 76, p. 162–174.

Holliday, V.T., 2004, Soils in Archaeological Research: Oxford, U.K., Oxford University Press, 464 p.

Holliday, V.T., Hovorka, S.D., and Gustavson, T.C., 1996, Lithostratigraphy and geochronology of fills in small playa basins on the Southern High Plains, United States: Geological Society of America, Bulletin, v. 108, p. 953–965.

Honey, J.G., Peláez-Campomanes, P., and Martin, R.A., 2005, Stratigraphic framework of early Pliocene fossil localities along the north bank of the Cimarron River, Meade County, Kansas: Ameghiniana, v. 42, p. 461–472.

Horwitz, P., and Knott, B., 1983, The burrowing habit of the koonac *Cherax plebejus* (Decapoda: Parastacidae): West Australian Naturalist, v. 15, p. 113–117.

Horwitz, P.H.J., Richardson, A.M.M., and Boulton, A., 1985, The burrow habitat of two sympatric species of land crayfish, *Engaeus urostrictus* and *E. tuberculatus* (Decapoda: Parastacidae): Victorian Naturalist, v. 102, p. 188–197.

Huerta, P., and Armenteros, I., 2005, Calcrete and palustrine assemblages on a distal alluvial-floodplain: a response to local subsidence (Miocene of the Duero basin, Spain): Sedimentary Geology, v. 177, p. 253–270.

Ibarra, D.E., Oster, J.L., Winnick, M.J., Caves Rugenstein, J.K., Byrne, M.P., and Chamberlain, C.P., 2018, Warm and cold wet states in the western United States during the Pliocene–Pleistocene, Geology, v. 46, p. 355–358.

IPCC, 2014, Climate Change 2014: Synthesis Report, Contribution of Working Groups I, II, and III to the Fifth Assessment Report of the Intergovernmental Panel on Climate Change: Geneva, Switzerland, Core Writing Team, R.K. Pachauri and L.A. Meyer, eds., 151 p.

Jenny, H., 1941, Factors of Soil Formation: A System of Quantitative Pedology: New York, McGraw-Hill, 281 p.

Jenny, H., 1994, Factors of Soil Formation: A System of Quantitative Pedology: Courier Corporation, 320 p.

Joeckel, R.M., Wooden, S.R., Korus, J.T., and Garbisch, J.O., 2014, Architecture, heterogeneity, and origin of late Miocene fluvial deposits hosting the most important aquifer in the Great Plains, USA: Sedimentary Geology, v. 311, p. 75–95.

Keighley, D.G., and Pickerill, R.K., 1995, Commentary: the ichnotaxa Palaeophycus and Planolites: historical perspectives and recommendations: Ichnos, v. 3, p. 301–309.

Kraus, M.J., 1987, Integration of channel and floodplain suites, II. Vertical relations of alluvial paleosols: Journal of Sedimentary Petrology, v. 57, p. 602–612.

Kraus, M.J., 1999, Paleosols in clastic sedimentary rocks: their geologic applications: Earth-Science Reviews, v. 47, p. 41–70.

Kretzschmar, A., 2004, Effects of Earthworms on Soil Organization, *in* Edwards, C.A., ed., Earthworm Ecology, Second Edition: Boca Raton, CRC press, p. 201–210.

Layzell, A.L., Mandel, R.D., Ludvigson, G.A., Rittenour, T.M., and Smith, J.J., 2015, Forces driving late Pleistocene (ca. 77–12 ka) landscape evolution in the Cimarron River valley, southwestern Kansas: Quaternary Research, v. 84, p. 106–117.

Lee, K.E., 1985, Earthworms: Their Ecology and Relationships with Soils and Land Use: Sydney, Academic Press, 411 p.

Leonard, E.M., 2002, Geomorphic and tectonic forcing of late Cenozoic warping of the Colorado piedmont: Geology, v. 30, p. 595–598.

Lindsay, E., Johnson, N.M., and Opdyke, N.D., 1975, Preliminary correlation of North American land mammal ages and geomagnetic chronology: Studies in cenozoic paleontology and stratigraphy: C.W. Hibbard Memorial, University of Michigan Museum of Paleontology, p. 111–119.

Lukens, W.E., Driese, S.G., Peppe, D.J., and Loudermilk, M., 2017a, Sedimentology, stratigraphy, and paleoclimate at the late Miocene Coffee Ranch fossil site in the Texas Panhandle: Palaeogeography, Palaeoclimatology, Palaeoecology, v. 485, p. 361–376.

Lukens, W.E., Lehmann, T., Peppe, D.J., Fox, D.L., Driese, S.G., and McNulty, K.P., 2017b, The Early Miocene Critical Zone at Karungu, Western Kenya: An Equatorial, Open Habitat with Few Primate Remains: Frontiers in Earth Science, v. 5, no. 87.

Lukens, W.E., Nordt, L.C., Stinchcomb, G.E., Driese, S.G., and Tubbs, J.D., 2018, Reconstructing pH of paleosols using geochemical proxies: Journal of Geology, v. 126, p. 427–449.

MacFarling Meure, C., Etheridge, D., Trudinger, C., Steele, P., Langenfelds, R., Van Ommen, T., Smith, A., and Elkins, J., 2006, Law Dome CO_2, CH_4 and N_2O ice core records extended to 2000 years BP, Geophysical Research Letters, v. 33, L14810.

Mack, G.H., James, W.C., and Monger, H.C., 1993, Classification of paleosols: Geological Society of America, Bulletin, v. 105, p. 129–136.

Marcolini, F., and Martin, R.A., 2008, Mosaic evolution in first lower molars of Pliocene *Ogmodontomys* (Rodentia: Arvicolidae) from the Meade Basin of southwestern Kansas (USA): Neues Jahrbuch für Geologie und Paläontologie, Abhandlungen, v. 249, p. 313–332.

Martin, R.A., 2003, Biochronology of latest Miocene through Pleistocene arvicolid rodents from the central Great Plains of North America: Coloquios de Paleontología, v. 1, p. 373–383.

Martin, R.A., and Peláez-Campomanes, P., 2014, Diversity dynamics of the Late Cenozoic rodent community from south-western Kansas: the influence of historical processes on community structure: Journal of Quaternary Science, v. 29, p. 221–231.

Martin, R.A., Honey, J.G., and Pelaez-Campomanes, P., 2000, The Meade Basin rodent project: a progress report: Paludicola, v. 3, p. 1–32.

Martin, R.A., Peláez-Campomanes, P., Honey, J.G., Fox, D.L., Zakrzewski, R.J., Albright, L.B., Lindsay, E.H., Opdyke, N.D., and Goodwin, H.T., 2008, Rodent community change at the Pliocene–Pleistocene transition in southwestern Kansas and identification of the *Microtus* immigration event on the Central Great Plains: Palaeogeography, Palaeoclimatology, Palaeoecology, v. 267, p. 196–207.

Martin, R.A., Peláez-Campomanes, P., Honey, J.G., Marcolini, F., and Akersten, W.A., 2011, Five million years of pocket gopher history in the Meade Basin of southwestern Kansas and northwestern Oklahoma: Journal of Vertebrate Paleontology, v. 31, p. 866–884.

Melchor, R.N., Genise, J.F., and Miquel, S.E., 2002, Ichnology, sedimentology and paleontology of Eocene calcareous paleosols from a palustrine sequence, Argentina: Palaios, v. 17, p. 16–35.

Merriam, D.F., and Mann, C.J., 1957, Sinkholes and related geologic features in Kansas: Kansas Academy of Science, Transactions, v. 60, p. 207–243.

Miall, A.D., 1978, Lithofacies types and vertical profile models in braided river deposits: a summary, *in* Miall, A.D., ed., Fluvial Sedimentology: Canadian Society of Petroleum Geology, Memoirs, v. 5, p. 597–604.

Miall, A.D., 2013, The Geology of Fluvial Deposits: Sedimentary Facies, Basin Analysis, and Petroleum Geology: Berlin, Springer, 582 p.

Montes, C., Cardona, A., Jaramillo, C., Pardo, A., Silva, J.C., Valencia, V., Ayala, C., Pérez-Angel, L.C., Rodriguez-Parra, L.A., and Ramirez, V., 2015, Middle Miocene closure of the Central American seaway: Science, v. 348, p. 226–229.

Osterkamp, W.R., and Wood, W.W., 1987, Playa-lake basins on the Southern High Plains of Texas and New Mexico: Part I. Hydrologic, geomorphic, and geologic evidence for their development: Geological Society of America, Bulletin, v. 99, p. 215–223.

Peláez-Campomanes, P., and Martin, R.A., 2005, The Pliocene and Pleistocene history of cotton rats in the Meade Basin of southwestern Kansas: Journal of Mammalogy, v. 86, p. 475–494.

Pemberton, S.G., and Frey, R.W., 1982, Trace fossil nomenclature and the *Planolites–Palaeophycus* dilemma: Journal of Paleontology, v. 56, p. 843–881.

Pound, M.J., Tindall, J., Pickering, S.J., Haywood, A.M., Dowsett, H.J., and Salzmann, U., 2014, Late Pliocene lakes and soils: a global data set for the analysis of climate feedbacks in a warmer world: Climate of the Past, v. 10, p. 167–180.

Prochnow, S.J., Atchley, S.C., Boucher, T.E., Nordt, L.C., and Hudec, M.R., 2006, The influence of salt withdrawal subsidence on palaeosol maturity and cyclic fluvial deposition in the Upper Triassic Chinle Formation: Castle Valley, Utah: Sedimentology, v. 53, p. 1319–1345.

Ravelo, A.C., Dekens, P.S., and McCarthy, M., 2006, Evidence for El Niño-like conditions during the Pliocene: GSA Today, v. 16, p. 4.

Ravelo, A.C., Lawrence, K.T., Fedorov, A., and Ford, H.L., 2014, Comment on "A 12-million-year temperature history of the tropical Pacific Ocean": Science, v. 346, p. 1467–1467.

Rawls, W.J., Brakensiek, D.L., and Saxtonn, K.E., 1982, Estimation of soil water properties: American Society of Agricultural Engineers, Transactions, v. 25, p. 1316–1320.

Retallack, G.J., 1994, A pedotype approach to latest Cretaceous and earliest Tertiary paleosols in eastern Montana: Geological Society of America, Bulletin, v. 106, p. 1377–1397.

Retallack, G.J., 2007, Cenozoic paleoclimate on land in North America: The Journal of Geology, v. 115, p. 271–294.

Retallack, G.J., 2008, Soils of the Past: An Introduction to Paleopedology, Second Edition: New York, John Wiley and Sons, 403 p.

Royer, D.L., 2016, Climate sensitivity in the geologic past: Annual Review of Earth and Planetary Sciences, v. 44, p. 277–293.

Schoeneberger, P.J., 2002, Field Book for Describing and Sampling Soils, Version 3.0: U.S. Government Printing Office, 286 p.

Schumm, S.A., and Lichty, R.W., 1963, Channel Widening And Flood-Plain Construction along Cimarron River in Southwestern Kansas: U.S. Government Printing Office, 88 p.

Seni, S.J., 1980, Sand-body geometry and depositional systems, Ogallala Formation, Texas: University of Texas, Austin, Bureau of Economic Geology, Report of Investigation 105, 36 p.

Sheldon, N.D., and Tabor, N.J., 2009, Quantitative paleoenvironmental and paleoclimatic reconstruction using paleosols: Earth-Science Reviews, v. 95, p. 1–52.

Sheldon, N.D., Retallack, G.J., and Tanaka, S., 2002, Geochemical climofunctions from North American soils and application to paleosols across the Eocene–Oligocene boundary in Oregon: The Journal of Geology, v. 110, p. 687–696.

Slade, N.A., Sauer, J.R., and Glass, G.E., 1984, Seasonal variation in field-determined growth rates of the hispid cotton rat (*Sigmodon hispidus*): Journal of Mammalogy, v. 65, p. 263–270.

Smith, J.J., and Hasiotis, S.T., 2008, Traces and burrowing behaviors of the cicada nymph *Cicadetta calliope*: neoichnology and paleoecological significance of extant soil-dwelling insects: Palaios, v. 23, p. 503–513.

Smith, J.J., Hasiotis, S.T., Woody, D.T., and Kraus, M.J., 2008, Paleoclimatic implications of crayfish-mediated prismatic structures in paleosols of the Paleogene Willwood Formation, Bighorn Basin, Wyoming, USA: Journal of Sedimentary Research, v. 78, p. 323–334.

Smith, J.J., Ludvigson, G.A., Layzell, A., Möller, A., Harlow, R.H., Turner, E., Platt, B., and Petronis, M., 2017, Discovery of Paleogene deposits of the central High Plains Aquifer in the western Great Plains, U.S.A.: Journal of Sedimentary Research, v. 87, p. 880–896. doi:10.2110/jsr.2017.48

Soil Survey Staff, 2014, Keys to Soil Taxonomy, 12th Edition: U.S. Department of Agriculture, Natural Resources Conservation Service, 360 p.

Soil Science Division Staff, 2017, Soil Survey Manual, Ditzler, C., Scheffe, K., and Monger, H.C., eds., U.S. Department of Agriculture, Handbook 18: Washington, D.C., U.S. Government Printing Office, 603 p.

Stinchcomb, G.E., Nordt, L.C., Driese, S.G., Lukens, W.E., Williamson, F.C., and Tubbs, J.D., 2016, A data-driven spline model designed to predict paleoclimate using paleosol geochemistry: American Journal of Science, v. 316, p. 746–777.

Tanner, L.H., 2000. Palustrine–lacustrine and alluvial facies of the (Norian) Owl Rock Formation (Chinle Group), Four Corners Region, Southwestern U.S.A: implications for Late Triassic paleoclimate: Journal of Sedimentary Research, v. 70, p. 1280–1289.

Tashiro, H., 1987, Turfgrass insects of the United States and Canada: Ithaca, New York, Cornell University Press, 448 p.

Taylor, D.W., 1960, Late Cenozoic molluscan faunas from the High Plains: U.S. Geological Survey, Professional Paper 337, 94 p.

Toonen, W.H., Kleinhans, M.G., and Cohen, K.M., 2012, Sedimentary architecture of abandoned channel fills: Earth Surface Processes and Landforms, v. 37, p. 459–472.

Vepraskas, M.J., 2001, Morphological features of seasonally reduced soils, *in* Richardson, J.L., and Vepraskas, M.J., eds., Wetland Soils: Genesis, Hydrology, Landscapes, and Classification: Boca Raton, Lewis Publishers, p. 163–82.

Welch, S.M., and Eversole, A.G., 2006, The occurrence of primary burrowing crayfish in terrestrial habitat: Biological Conservation, v. 130, p. 458–464.

White, J., and Strehl, C.E., 1978, Xylem feeding by periodical cicada nymphs on tree roots: Ecological Entomology, v. 3, p. 323–327.

Wiest, L.A., Lukens, W.E., Peppe, D.J., Driese, S.G., and Tubbs, J., 2018, Terrestrial evidence for the Lilliput effect across the Cretaceous–Paleogene (K-Pg) boundary: Palaeogeography, Palaeoclimatology, Palaeoecology, v. 491, p.161–169.

Wilding, L.P., and Rehage, J.A., 1985, Pedogenesis of soils with aquic moisture regimes, *in* Wetland Soils: Characterization, Classification, and Utilization: International Rice Research Institute, Los Baños, Philippines p. 139–157.

Williner, V., Carvalho, D.A., and Collins, P.A., 2014, Feeding spectra and activity of the freshwater crab *Trichodactylus kensleyi* (Decapoda: Brachyura: Trichodactylidae) at La Plata basin: Zoological Studies, v. 53, no. 71.

Winnick, M.J., Welker, J.M., and Chamberlain, C.P., 2013, Stable isotopic evidence of El Niño-like atmospheric circulation in the Pliocene western United States: climate of the past, v. 9, p. 903–912.

Wood, W.W., and Osterkamp, W.R., 1987, Playa-lake basins on the Southern High Plains of Texas and New Mexico: Part II. A hydrologic model and mass-balance arguments for their development: Geological Society of America, Bulletin, v. 99, p. 224–230.

Wright, V.P., and Platt, N.H., 1995, Seasonal wetland carbonate sequences and dynamic catenas: a re-appraisal of palustrine limestones: Sedimentary Geology, v. 99, p. 65–71.

Yaalon, D.H., 1971, Paleopedology; Origin, Nature, and Dating of Paleosols: International Society of Soil Science and Israel Universities Press, Jerusalem, 350 p.

Zakrzewski, R.J., 1975, Pleistocene stratigraphy and paleontology in western Kansas; the state of the art, *in* Smith, G.R., and Friedland, N.E., eds., Studies on Cenozoic Paleontology and Strartigraphy: C.W. Hibbard Memorial, University of Michigan Museum of Paleontology, p. 121–128.

Zamanian, K., Pustovoytov, K., and Kuzyakov, Y., 2016, Pedogenic carbonates: forms and formation processes: Earth-Science Reviews, v. 157, p. 1–17.

Received 23 April 2018; accepted 17 January 2019.